ANALYSIS AND IMPLEMENTATION OF PREDICTION MODELS FOR THE DESIGN OF FIXED TERRESTRIAL POINT-TO-POINT SYSTEMS

A THESIS SUBMITTED TO

THE GRADUATE SCHOOL OF ENGINEERING AND SCIENCE

OF BILKENT UNIVERSITY

IN PARTIAL FULFILLMENT OF THE REQUIREMENTS FOR

THE DEGREE OF

MASTER OF SCIENCE

IN

ELECTRICAL AND ELECTRONICS ENGINEERING

By

Polat Göktaş

January, 2015

ANALYSIS AND IMPLEMENTATION OF PREDICTION MODELS FOR THE DESIGN OF FIXED TERRESTRIAL POINT-TO-POINT SYSTEMS

By Polat Göktaş

January, 2015

We certify that we have read this thesis and that in our opinion it is fully adequate, in scope and in quality, as a thesis for the degree of Master of Science.

Prof. Dr. Ayhan Altıntaş (Advisor)

Prof. Dr. Ezhan Karaşan

Assist. Prof. Dr. Satılmış Topcu

Approved for the Graduate School of Engineering and Science:

Prof. Dr. Levent Onural
Director of the Graduate School

ABSTRACT

ANALYSIS AND IMPLEMENTATION OF PREDICTION MODELS FOR THE DESIGN OF FIXED TERRESTRIAL POINT-TO-POINT SYSTEMS

Polat Göktaş
M.S. in Electrical and Electronics Engineering
Advisor: Prof. Dr. Ayhan Altıntaş
January, 2015

In this study, propagation link analysis and implementation of prediction models for the design of fixed terrestrial point-to-point systems are aimed. Different propagation models in the literature are examined as case studies and comparisons are made. Rec. ITU-R P.530 Model is analyzed in detail. The worst month link availability is investigated for terrestrial microwave LOS/NLOS radio links operating in NATO Band 3+ (1350-2690 MHz) and NATO Band 4 (4400-5000 MHz) frequency bands. The calculation of Bullington model of diffraction loss is extended for LOS path case and determination of reflection points on the terrain profile is improved. Several terrestrial microwave LOS/NLOS radio links are analyzed using the propagation parameters such as TX (transmitter) and RX (receiver) station coordinates, path length, frequency, antenna heights above ground level, antenna gains, polarization, radio refractivity gradient, time percentage, target SNR (Signal to Noise Ratio), bandwidth, digital terrain elevation and climate data. The calculation of the received power with the effect of the ground reflection is developed to calculate the fade margin in the defined microwave LOS/NLOS radio links. Received power is calculated by taking into consideration the attenuation due to rain and atmospheric gases, diffraction loss and the effect of multipath fading due to reflection. The validity of the implementation of link analysis is justified by comparison with the commercial ATDI ICS telecom software and the measurement data existing in the literature over sample microwave LOS/NLOS radio links.

Keywords: Rec. ITU-R P.530, multipath fading, link availability, received power, line-of-sight (LOS) and non line-of-sight (NLOS) microwave radio links.

ÖZET

SABİT KARASAL NOKTADAN-NOKTAYA SİSTEMLERİNİN TASARIMI İÇİN TAHMİN MODELLERİNİN ANALİZİ VE UYGULANMASI

Polat Göktaş
Elektrik ve Elektronik Mühendisliği Bolumu, Yüksek Lisans
Tez Danışmanı: Prof. Dr. Ayhan Altıntaş
Ocak, 2015

Bu çalışmada, sabit karasal noktadan-noktaya sistemlerin tasarımı için yayılım tahmin modellerinin link analizi ve uygulanması amaçlanmıştır. Literatürdeki farklı yayılım modellerinin simülasyon çalışması olarak incelenmesi ve karşılaştırması yapılmıştır. Detaylı olarak, ITU-R P.530 modeli analiz edilmiştir. NATO Band 3+ (1350-2690 MHz) ve 4 (4400-5000 MHz) frekans bandında çalışan karasal mikrodalga radyo LOS/NLOS (Görüş çizgisinin üstünde/altında) linkleri için yayılım mekanizmalarınn en kötü aydaki link kullanılabilirliği araştırılmıştır. Kama kırınım kaybında, Bullington modeli hesabının LOS arazi için genişletilmesi ve arazi hat profilindeki yansıma noktalarının bulunması geliştirilmiştir. TX (verici) ve RX (alıcı) istasyonların koordinat bilgileri, radyo linkin TX ve RX istasyonlar arasındaki mesafesi, frekans, TX ve RX antenlerin yerden yükseklikleri ve kazançları, polarizasyon tipi, radyo kırılma indisi, zaman yüzdesi, hedef SNR (sinyal gürültü oranı), bant genişliği, sayısal arazi yükseklik haritası ve iklimsel veriler gibi yayılım parametreleri kullanılarak çeşitli karasal mikrodalga LOS/NLOS radyo linkler için analizler edilmiştir. LOS/NLOS mikrodalga radyo linklerinde sönümlenme kesintisini hesaplamak için yerden yansımanın etkisi ile alıcıdaki güç seviyesinin hesaplanması geliştirilmiştir. Yağmur ve atmosferik gazlardan kaynaklanan zayıflama, yansımadan kaynaklanan çok yollu sönümlenmenin etkisi ve kama kırınım kaybı dikkate alınarak alıcıdaki güç seviyesi hesaplanmıştır. Link analizi uygulanmasının doğrulanması, örnek mikrodalga LOS/NLOS radyo linklerinde ticari ATDI ICS telecom yazılımı ve literatürde yer alan ölçüm verileri ile kıyaslanarak yapılmıştır.

Anahtar sözcükler: ITU-R P.530, çok yollu sönümlenme, link kullanılabilirliği, alıcıdaki güç seviyesi, karasal görüş çizgisi ve ufuk ötesi mikrodalga radyo linkleri.

Acknowledgement

First and foremost, I would like to sincerely extend my greatest appreciation to my supervisor, Prof. Dr. Ayhan Altıntaş, for his guidance, constructive criticism, advice and encouragement throughout my masters program.

It is a pleasure to express my special thanks to Prof. Dr. Ezhan Karaşan and Assist. Prof. Dr. Satılmış Topcu for their invaluable contributions of this thesis, and also for supplying significant resources for the development of this thesis at Communication and Spectrum Management Research Center (ISYAM). I would also like to thank Mr. Gökhan Moral for their cooperation and friendship.

I wish to thank all of my friends and family members for their continuous support and encouragement.

I was personally supported by TUBITAK, through BIDEB 2228 scholarship.

Contents

1 INTRODUCTION **1**

2 REVIEW OF MULTIPATH FADING MODELS **4**

2.1 Overview of Multipath Fading Models 4

2.1.1 Barnett-Vigants Model 5

2.1.2 Morita Model 7

2.1.3 Rec. ITU-R P.530 Model 8

2.2 Comparison of Multipath Fading Models 10

2.3 Case Studies for Multipath Fading Models 13

3 PROPAGATION MECHANISMS ON TERRESTRIAL MICROWAVE RADIO LINK **17**

3.1 Atmospheric Effects on Propagation 18

3.1.1 Attenuation due to Atmospheric Gases 19

3.1.2 Attenuation due to Rain 20

3.2 Diffraction Fading 26

3.2.1 Single Knife-Edge Diffraction Model 26

3.2.2 Double Knife-Edge Diffraction Model 30

3.2.2.1 Deygout Method 31

3.2.2.2 Epstein-Peterson Method 32

3.2.3 Multiple Knife-Edge Diffraction Model 33

3.2.3.1 Delta-Bullington Method 33

3.2.3.2 Proposed Diffraction Method 36

3.3 Diffuse Reflection Loss 38

4 LINK ANALYSIS AND SIMULATION STUDIES 43

4.1 Link Power Budget 44

4.1.1 Free Space Loss 45

4.1.2 Received Power 46

4.1.3 Noise Power 46

4.1.4 Coherence Bandwidth 47

4.1.5 Fade Margin 48

4.1.6 Link Availability 48

4.2 Path Profile and Simulation Studies 49

4.2.1 Kazan-Elmadag Microwave R/L Case Study 51

4.2.2 Fenertepe-Sazlıtepe Microwave R/L Case Study 55

4.2.3 Polatlı-Hüseyingazi Microwave R/L Case Study 58

4.2.4 Dikmen-Polatlı Microwave R/L Case Study 62

5 VALIDATION AND COMPARISON OF RESULTS 65

5.1 Comparison with the ATDI ICS Telecom Software 66

5.2 Experimental Validation of ITU-R Model for Terrestrial LOS/NLOS Microwave Links 69

6 CONCLUSION 73

A Effective Earth Radius 76

B Fresnel Zones 81

List of Figures

2.1 Barnett-Vigants atmospheric propagation conditions map for the United States. 6

2.2 Worldwide map of Barnett-Vigants atmospheric propagation conditions. 6

2.3 Refractivity gradient in the lowest 65 m of the atmosphere not exceeded for 1% of the average year, dN_1. 9

2.4 Map of the world showing countries for which data are available in the ITU-R database. 11

2.5 Cumulative distributions of error for the 239 links (including overland and overwater links) ITU-R P. 530-8 model (——); Barnett-Vigants model(- - -); Morita model(–. –. –.). 12

2.6 Terrain path profile of Fenertepe-Sazlıtepe microwave LOS radio link (the blue curve and the red curve indicate the first Fresnel zone and the 0.6 First Fresnel zone, respectively). 14

2.7 Percentage of time that fade depth has exceeded in the worst month for various multipath fading models, 1.350 GHz. 15

2.8 Percentage of time that fade depth has exceeded in the worst month for various multipath fading models, 5 GHz. 16

3.1 Specific attenuation due to atmospheric gases: atmospheric pressure, 1013 hPa; temperature, 15^o C; water vapour, 7.5 g/m^3. . . . 20

3.2 Rain attenuation prediction procedure. 22

3.3 Specific attenuation due to rain for Sarıyer-Maslak radio link. . . 23

3.4 Specific attenuation due to rain for Polatlı-Elmadag radio link. . . 23

3.5 Rain attenuation on terrestrial 5 GHz link as a function of vertical polarization. 25

3.6 Rain attenuation on terrestrial 5 GHz link as a function of horizontal polarization. 25

3.7 Shadowing of radio waves by an object. 28

3.8 Illustration of different single knife-edge diffraction scenarios. (a) NLOS path case and α_1, α_2 and v are positive, since h is positive (b) LOS path case and α_1, α_2 and v are negative, since h is negative. 28

3.9 Knife-edge diffraction loss as a function of Fresnel knife-edge diffraction parameter. 29

3.10 Knife-edge diffraction loss as a function of normalized clearance. . 29

3.11 Deygout method geometry over the LOS line. 32

3.12 Epstein-Peterson method geometry over the LOS line. 33

3.13 Bullington method geometry over the LOS line. 36

3.14 Relative permittivity, ε_r and conductivity, σ (S/m) as a function of frequency. 39

3.15 The geometry of the reflected propagation path. 41

4.1 An illustration of a typical microwave radio link. 44

4.2 Location of sites used for microwave link simulations in Istanbul. . 50

4.3 Location of sites used for microwave link simulations in Ankara. . 50

4.4 Terrain path profile of Kazan-Elmadag microwave LOS radio link (Frequency: 2 GHz, TX&RX Antenna Heights: 15 m a.g.l). 51

4.5 Terrain path profile of Polatlı-Hüseyingazi microwave NLOS radio link (Frequency: 1.35 GHz, TX&RX Antenna Heights: 35 m a.g.l). 58

4.6 Terrain path profile of Dikmen-Polatlı microwave NLOS radio link (Frequency: 2.690 GHz, TX&RX Antenna Heights: 40 m a.g.l). . 62

5.1 Kazan-Elmadag microwave LOS radio link profile over terrain with the terrain elevations above sea level adjusted for 4/3 effective Earth radius curvature by the ATDI ICS telecom software. 66

5.2 Terrain path profile of the scenario 1 (Frequency: 5 GHz, TX Antenna Height: 9.8 m a.g.l and RX Antenna Height: 4.6 m a.g.l). 70

5.3 Terrain path profile of the scenario 2 (Frequency: 2 GHz, TX Antenna Height: 11.8 m a.g.l and RX Antenna Height: 35 m a.g.l). 70

5.4 Path loss for the scenario 1 as abtained during the measurements and by using the Delta-Bullington diffraction method for the transmitter antenna height of 9.8 m a.g.l. 71

5.5 Path loss for the scenario 2 as abtained during the measurements and by using the Delta-Bullington diffraction method for the transmitter antenna height of 11.8 m a.g.l. 72

5.6 Path loss for the scenario 2 as abtained during the measurements and by using the Delta-Bullington diffraction method for the transmitter antenna height of 23.8 m a.g.l. 72

A.1 Variation of the ray curvature for different values of k. 78

A.2 Polatlı-Elmadag microwave radio link profile over terrain with the terrain elevations above sea level adjusted for 4/3 effective Earth radius curvature. (the blue curve and the red curve indicate the first Fresnel zone and the 0.6 first Fresnel zone, respectively). . . . 80

B.1 Geometrical concept of Fresnel zones. 83

B.2 An illustration of the first Fresnel zone radius. 83

List of Tables

2.1 Error statistics for various multipath fading models in terms of terrain-climatic grouping of the links. 11

2.2 Percentage of links with error not exceeded in certain ranges. . . . 12

2.3 Terrestrial link parameters for Fenertepe-Sazlıtepe propagation path. 14

2.4 Comparison of derived parameters for three multipath fading models on Fenertepe-Sazlıtepe microwave LOS radio link 15

3.1 Path propagation parameters used in Rec. ITU-R P.530 and P.526. 18

3.2 Main parameters used for reflection case study. 40

3.3 The values of conductivity and relative permittivity for different types of ground at 2 GHz frequency. 41

3.4 Reflection case study results for different types of ground and vertical polarization on Fenertepe-Sazlıtepe microwave LOS link. . . 41

3.5 Reflection case study results for different types of ground and horizontal polarization on Fenertepe-Sazlıtepe microwave LOS link. . 42

4.1 The outage time per year allowed for given link availability. 49

4.2 Terrestrial link parameters for Kazan-Elmadag microwave LOS radio link. 52

4.3 Results of link simulation as a function of vertical polarization on Kazan-Elmadag terrestrial microwave LOS radio link. 53

4.4 Results of link simulation as a function of horizontal polarization on Kazan-Elmadag terrestrial microwave LOS radio link. 54

4.5 Terrestrial link parameters for Fenertepe-Sazlıtepe microwave LOS radio link. 55

4.6 Results of link simulation as a function of vertical polarization on Fenertepe-Sazlıtepe terrestrial microwave LOS radio link. 56

4.7 Results of link simulation as a function of horizontal polarization on Fenertepe-Sazlıtepe terrestrial microwave LOS radio link. . . . 57

4.8 Terrestrial link parameters for Polatlı-Hüseyingazi microwave NLOS radio link. 59

4.9 Results of link simulation for both horizontal and vertical polarizations on Polatlı-Hüseyingazi terrestrial microwave NLOS radio link (by using only Delta-Bullington diffraction method). 60

4.10 Results of predicted diffraction loss for three diffraction prediction methods on Polatlı-Hüseyingazi terrestrial microwave NLOS radio link. 61

4.11 Results of predicted received power for three diffraction prediction methods on Polatlı-Hüseyingazi terrestrial microwave NLOS radio link. 61

4.12 Terrestrial link parameters for Dikmen-Polatlı microwave NLOS radio link. 63

4.13 Results of link simulation for both horizontal and vertical polarizations on Dikmen-Polatlı terrestrial microwave NLOS radio link. 64

5.1 Terrestrial link parameters for Kazan-Elmadag terrestrial microwave LOS radio link (validation case study). 67

5.2 Results of link simulation as a function of vertical polarization on Kazan-Elmadag terrestrial microwave LOS radio link (validation case study). 68

5.3 Results of ATDI ICS telecom software on Kazan-Elmadag terrestrial microwave LOS radio link. 68

5.4 Selected measurement scenarios. 69

5.5 System parameters at 2.0 GHz, 3.5 GHz and 5.0 GHz. 69

A.1 k factor values for different atmospheric refractive conditions. . . 79

Chapter 1

INTRODUCTION

In fixed point-to-point microwave radio links, the information is transmitted between transmitting and receiving antennas by electromagnetic waves. The signal strength of electromagnetic waves weakens during wave propagation through the environment. The difference of signal strengths from transmitter to receiver sites is called as propagation path loss. The major mechanisms in path loss are attenuation due to atmospheric absorption, attenuation due to rain, diffraction loss due to obstructions and multipath fading due to multipath arising from reflection points along the terrain path profile in addition to the free space path loss. The fade margin is derived from the link budget calculation, and this parameter is then used to find the link availability in the terrestrial microwave LOS/NLOS radio link. Link availability is the main design parameter for many fixed terrestrial microwave radio links.

In the literature, prediction models for deep-fading range of the multipath fading distribution have been in existence for several years. Most of these have been based on empirical fits of Rayleigh-type distributions (i.e., with slopes of 10 dB/decade) to the fading data for individual countries. The best known techniques in this category are those of Morita [1] for Japan (actually a worst-season technique), Barnett [2] and Vigants [3] for the United States. Olsen and Tjelta paper [4,5] have presented detailed testing results for the ITU-R P.530-8 model [6]

on a 239-link database from 22 countries around the world in comparison with the results for the leading regional methods still frequently used by some link designers for worldwide applications (the Barnett-Vigants model [2] of the United States and the Morita model [1] of Japan).

In this study, we have investigated the performance of various "Point-to-Point" path loss models on terrestrial microwave LOS/NLOS radio links in NATO Band 3+ (1350-2690 MHz) and NATO Band 4 (4400-5000 MHz) frequency ranges. A total of three multipath fading models, namely Barnett-Vigants [2,3], Morita [1] and Rec. ITU-R P.530 [7] models have been reviewed with different terrestrial link and geoclimatic parameters in a rural environment. All estimated results of the considered models are compared with the Rec. ITU-R P.530 [7] model values. The available signal power formulation at the receiver with the effect of the ground reflection is developed in the terrestrial microwave LOS/NLOS radio links. Then, we calculated the fade margin in order to find the link availability value.

In Chapter 2, we have made a comparative study between three commonly used prediction models for the terrestrial microwave LOS/NLOS radio links: Barnett-Vigants [2, 3], Morita [1] and Rec. ITU-R P.530 [7]. We have analyzed the link unavailability as a function of various parameters such as frequency, fade margin and path distance. In addition, we have compared the performance of the three multipath fading models in terms of the total outage probability over the sample microwave radio link.

Chapter 3 presents work on the evaluation of the Rec. ITU-R P.530 point-to-point radiowave propagation prediction model [7]. Four main aspects are analyzed: attenuation due to atmospheric gases and rain, the signal attenuation due to diffraction based on knife-edge obstruction, and multipath fading due to multipath arising from specular reflection points along the terrestrial microwave radio links.

Chapter 4 describes the implementation of the above mentioned Rec. ITU-R P.530 model [7], and includes simulation results and performance evaluations over sample fixed terrestrial microwave LOS/NLOS radio links. Then, the values of

the total received power and fade margin are calculated in the defined terrestrial microwave LOS/NLOS radio link. The impact of several sites and environmental parameters are examined in the calculation of the total received power.

In Chapter 5, the implementation of link analysis is compared by using both the commercial ATDI ICS telecom software [8] and the measurement data existing in the literature [9, 10] over sample fixed terrestrial microwave LOS/NLOS radio links. Concluding remarks and future works are discussed in Chapter 6.

Appendix A provides an information about k factor values for different atmospheric refractive conditions, and also indicates the calculation of the radio refractivity, dN_1 (N-units/km) that is point refractivity gradient in the lowest 65 m of the atmosphere not exceeded for 1% of an average year.

Appendix B gives an information about Fresnel zone and ellipsoid in order to calculate the diffraction loss along the terrestrial microwave radio LOS/NLOS link, and the clearance criteria is then defined in the terrestrial microwave LOS/NLOS radio link. So, the direct path between the transmitter and receiver sites needs a clearance above ground of at least 60% of the radius of the first Fresnel zone to achieve free space propagation condition.

Chapter 2

REVIEW OF MULTIPATH FADING MODELS

Propagation prediction models for the design of fixed terrestrial point-to-point systems have been derived estimating the probability of outage and link availability over a period of time. This chapter focuses on reviewing multipath fading models as adopted by different authors in the worldwide. This chapter is divided into two sections. The first section summarizes multipath fading models taking into account different geoclimatic and terrestrial link parameters. The second section compares the performance of all multipath fading models in terms of total outage probability over the sample fixed terrestrial microwave radio link.

2.1 Overview of Multipath Fading Models

Techniques for predicting the deep-fading range of the multipath fading distribution have been available for several years. Three models are commonly used to predict the worst month link unavailability in the terrestrial microwave LOS/ NLOS radio links as called Morita [1], Barnett-Vigants [2, 3] models used respectively in Japan, North America, and the worldwide Rec. ITU-R P.530 model [7].

2.1.1 Barnett-Vigants Model

The Barnett-Vigants fading model was based on the published work of two microwave system researchers at AT&T Bell Labs [2, 3]. This work was defined as a regional model to create semi-emprical equations for a fade of depth probability of the received signal. Barnett-Vigants fading model depends mainly on climate factor in the USA. The worst month probability of a fade of depth, A is given by [11, 12]:

$$p = 6 \times 10^{-7} C f d^3 10^{-A/10} \quad \% \tag{2.1}$$

where

d is the path distance between the transmitter and receiver sites in km,

f is the radio frequency in GHz,

C is the propagation conditions factor,

A is the fade depth in dB.

The propagation conditions factor is selected on the basis of the type of environment in which the link is to operate. Barnett-Vigants atmospheric propagation conditions maps [11] for both the United States and around the worldwide are shown in Fig. 2.1 and 2.2.

The propagation conditions factor, C where equals [2, 3]:

$$C = \begin{cases} 0.25 & for\ mountains\ and\ dry\ climate \\ 1 & for\ average\ terrain\ and\ climate \\ 4 & for\ over\ water \end{cases}$$

According to the Fig. 2.2, we have observed that the propagation conditions factor for Barnett-Vigants multipath fading model could not consider any variations over Turkey. In accordance with Ericssonwide Internal Report [13], the path inclination parameter is found to be extremely siginificant parameter in the design of fixed terrestrial microwave radio links. However, it is not included in the Barnett-Vigants multipath fading model [2, 3] to calculate the worst month link unavailability in the fixed terrestrial microwave radio link.

Figure 2.1: Barnett-Vigants atmospheric propagation conditions map for the United States.

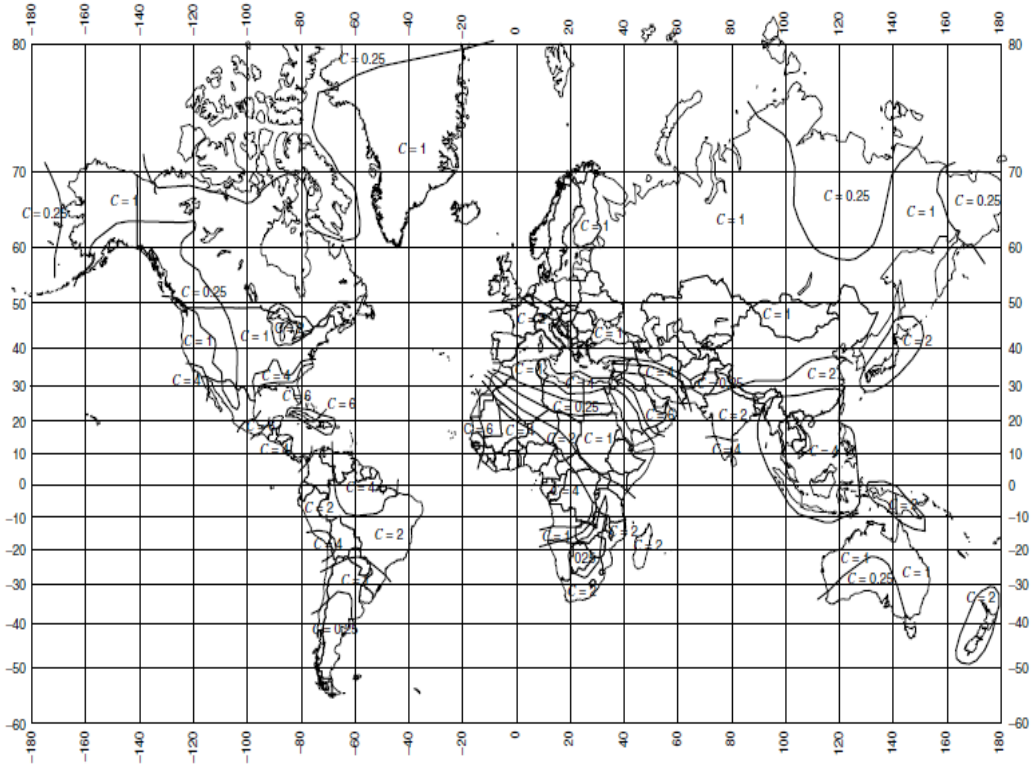

Figure 2.2: Worldwide map of Barnett-Vigants atmospheric propagation conditions.

2.1.2 Morita Model

Kazuo Morita [1] derived an empirical formulation for the Rayleigh fading occurrence probability of line-of-sight microwave radio links as a result of propagation tests in the worst month case for many years in Japan. Rayleigh fading occurrence probability was obtained by using a lot of fading data measured on propagation test paths. In addition, measured Rayleigh fading occurrence probability was taken in the 4 and 6 GHz microwave links on a hop between Tokyo-Osaka. He also presented geoclimatic variability by proving propagation geoclimatic factor for three regions namely: plain, over water and mountainous regions [14]. The empirical formulation depends on path distance, path height and inclination of the defined propagation path. The following empirical formula gives of the occurrence probability of Rayleigh fading as a result of propagation tests for many years [1]:

$$p = (f/4)^{1.2} Q d^{3.5} 10^{-A/10} \quad \% \tag{2.2}$$

where

d is the path distance between the transmitter and receiver sites in km,

f is the radio frequency in GHz,

Q is the propagation geoclimatic factor,

A is the fade depth in dB.

Geoclimatic factor values of the propagation path become as follows [1]:

$$Q = \begin{cases} 2.0 \times 10^{-9} & for\ over\ the\ mountains \\ 5.1 \times 10^{-9} & for\ over\ the\ plains \\ 3.7 \times 10^{-7}\sqrt{1/\sqrt{h}} & for\ over\ water \end{cases}$$

where h is the average path height along the terrain path profile in meters.

2.1.3 Rec. ITU-R P.530 Model

Rec. ITU-R P.530 [7] is one of the most widely used model providing guidelines for the design of terrestrial microwave LOS/NLOS radio links. A worldwide fading model has been recommended by the Radiocommunication Sector of the International Telecommunication Union (ITU-R) Study Group 3. The Study Group 3 of ITU has continued to revise the ITU-R P.530 models since the first version of 1978 [15, 16]. This recommendation is used to predict path losses in the average worst month for terrestrial microwave LOS/NLOS radio links. The worst month link unavailability depends on the impacts of both climate and terrain datas. Two possible parameters are discussed below to calculate the geoclimatic factor for the terrestrial microwave LOS/NLOS radio link.

S_a is defined as the standard deviation of terrain heights (m) within a 110 km $\times$ 110 km area mentioned in Rec. ITU-R P.530. The worldwide data for this parameter is provided by ITU-R Study Group 3. The worldwide S_a data provided by ITU-R is too coarse such that the distance between grid points is 110 km. If the path length between transmitter and receiver sites is less than 110 km, terrain roughness parameter is computed by using bi-linear interpolation at the four closest gridpoints. The data provided by ITU-R Study Group 3 is also too coarse to find the geoclimatic factor for the terrestrial microwave radio link [17].

The another required parameter is the radio refractivity gradient, dN_1 that is the point refractivity gradient in the lowest 65 m of the atmosphere not exceeded for 1% of an average year. The radio refractivity parameter is provided on a 1.5 grid in latitude and longitude in Rec. ITU-R P.453 [18]. The refractivity gradient in the lowest 65 m of the atmosphere, dN_1 for the worldwide is shown in Fig. 2.3.

There are two ways to calculate geoclimatic factor parameter: a quick calculation (QC) and a detailed link design (DLD) methods [7].

- The quick calculation (QC) method uses only dN_1, point refractivity gradient parameter. The worst month outage probability, p_w depends on the geoclimatic factor of the quick calculation method according to Eq. (2.5).

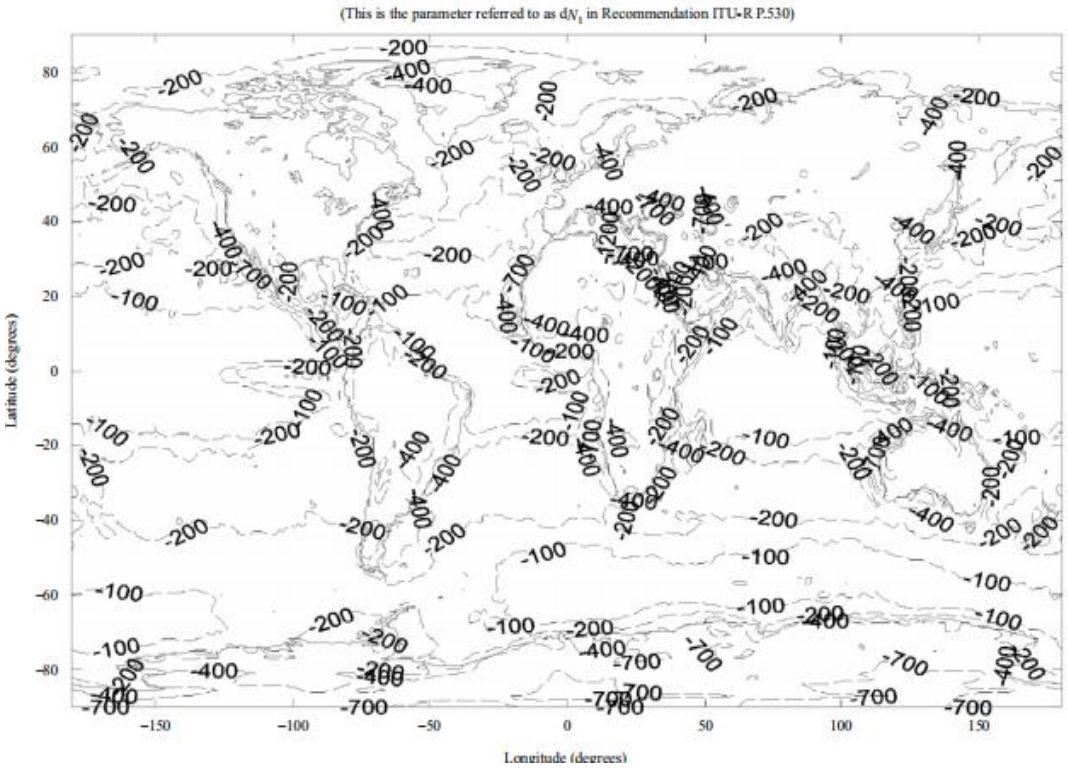

Figure 2.3: Refractivity gradient in the lowest 65 m of the atmosphere not exceeded for 1% of the average year, dN_1.

ITU-R P.530-15 Fading Prediction Model

$$\mathrm{K}=10^{-4.6-0.0027dN_1} \tag{2.3}$$

$$p_o = Kd^{3.1}(1+|\varepsilon_p|)^{-1.29} f^{0.8} \times 10^{-0.00089h_L} \tag{2.4}$$

$$p_w = p_o \times 10^{\frac{-A}{10}} \quad \% \tag{2.5}$$

- dN_1 and S_a parameters are needed to calculate the geoclimatic factor of the detailed link design (DLD) method. The percentage of time that fade depth, A (in decibels) is exceeded in the average worst month calculated as:

$$\mathrm{K}= 10^{-4.4-0.0027dN_1}(10+S_a)^{-0.46} \tag{2.6}$$

$$p_o = Kd^{3.4}(1+|\varepsilon_p|)^{-1.03} f^{0.8} \times 10^{-0.00076h_L} \tag{2.7}$$

$$p_w = p_o \times 10^{\frac{-A}{10}} \quad \% \tag{2.8}$$

where

d is the path distance between the transmitter and receiver sites in km,

f is the radio frequency in GHz,

K is the geoclimatic factor,

ϵ_p is the path inclination in mrad,

h_L is the altitude of the lower transmitter or receiver site in meters, a.s.l.

The parameters dN_1, S_a, $|\varepsilon_p|$ and h_L significantly affect the fade occurrence factor, p_o and the link unavailability due to multipath fading probability, p_w. Eq. (2.4) and (2.7) are used for small percentages of time, but A must be replaced by A_t, the fade depth at which the transition occurs between deep-fading and shallow-fading distribution for all percentages of time.

Rec. ITU-R P.530 model depends on path data, climate and terrain parameters when compared with the other multipath fading models [15]. The propagation geoclimatic factor of this model varies based on refractivity gradient and terrain roughness parameters over Turkey.

2.2 Comparison of Multipath Fading Models

In accordance with Olsen-Tjelta [4, 5] and Ericssonwide Internal Report [13] papers, the application of three models for many regions around the world clearly shows that the ITU-R model [7] gives the best overall performance in modeling flat-fading statistics on overland links and also on links in rugged inland regions. A multipath fading data base based on the ITU-R databese having 239 links (206 overland and 33 overwater) in 22 countries for frequencies ranging from 450 MHz to 37 GHz located in regions from mountains to over water. A map showing the geographical distribution of data is given in Fig. 2.4, and the error statistics for three fading models in terms of terrain grouping of the links is shown in Table. 2.1. In Table 2.2 shows which percent of 239 links not exceeded the range of these errors.

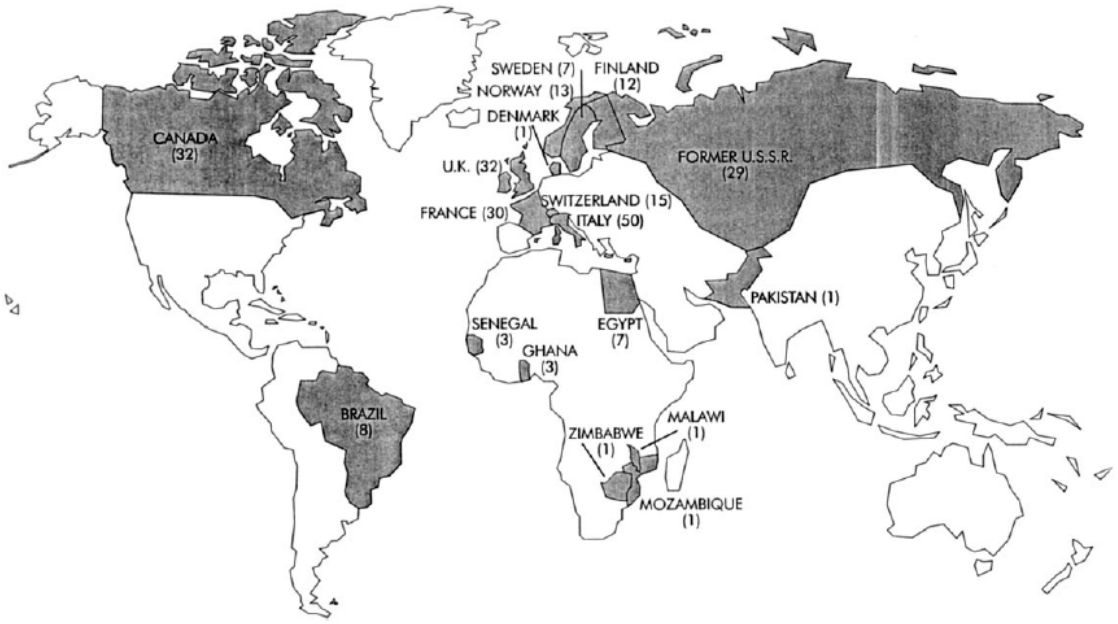

Figure 2.4: Map of the world showing countries for which data are available in the ITU-R database.

Link Grouping	N	<E>(dB)			σ_E (dB)			RMS (dB)			% $\lvert E - <E> \rvert$ >10 (dB)		
		ITU-R	US	JPN	ITU-R	US	JPN	ITU-R	US	JPN	ITU-R	US	JPN
ITU-R Inland	111	0.1	2.8	-12.1	5.2	6.6	7.7	5.3	9.4	19.8	3.6	12.6	13.5
US Inland	104	0.0	2.4	-12.5	5.3	6.7	7.5	5.4	9.1	20.1	4.8	13.5	13.5
JPN Island	122	0.1	2.7	-12.3	5.4	6.6	7.4	5.5	9.3	19.8	4.9	12.3	13.1
ITU-R Mountainous	37	0.3	5.8	-6.6	6.2	8.2	8.2	6.4	14.1	14.9	8.1	21.6	21.6
US/JPN Mountainous	44	0.7	6.3	-6.0	5.9	7.8	7.8	6.6	14.2	13.9	6.8	18.2	18.2
ITU-R Coastal (medium-sized)	10	-2.2	2.3	-11.3	5.5	5.6	5.3	7.8	8.0	17.2	0.0	10.0	10.0
ITU-R Coastal (large)	38	0.1	2.4	-11.4	4.6	5.9	5.3	4.7	8.3	16.8	2.6	5.3	7.9
ITU-R Coastal	58	-1.0	1.9	-11.8	4.9	5.6	5.1	5.9	7.6	16.9	3.5	6.9	6.9
JPN Coastal	40	-1.9	0.8	-12.5	3.8	4.4	3.5	5.7	5.2	16.2	0.0	2.5	0.0
ITU-R Overwater (medium-sized)	6	7.3	7.9	-1.9	5.4	6.1	6.8	13.4	14.8	8.9	0.0	0.0	0.0
ITU-R Overwater (large)	21	0.9	-0.8	-12.0	8.2	9.9	11.2	9.2	10.8	23.5	23.8	28.6	28.6
ITU-R Overwater	27	2.4	1.1	-9.8	8.1	9.8	11.1	10.5	11.0	21.1	22.2	22.2	29.6
ITU-R Coastal/Overwater (medium-sized)	16	1.4	4.4	-7.8	7.1	6.2	7.4	8.5	10.8	15.4	18.8	12.55	18.8
ITU-R Coastal/Overwater (large)	59	0.4	1..3	-11.6	6.1	7.6	7.8	6.5	8.9	19.5	8.5	11.9	15.3
ITU-R Coastal/Overwater	85	0.1	1.7	-11.2	6.2	7.2	7.5	6.3	8.9	18.7	10.6	12.9	15.3
US Coastal/Overwater	84	0.0	1.6	-11.4	6.1	7.0	7.5	6.2	8.6	19.0	8.3	10.7	13.1
JPN Coastal/Overwater	67	-0.2	1.0	-11.4	6.2	7.0	7.6	6.4	8.0	19.1	9.0	10.5	13.4
High lat. ($\geq 60_o$)	28	*0.3	0.8	-11.9	8.6	9.6	10.9	9.0	10.4	23.0	21.4	17.9	28.6
All overland	206	-0.2	3.1	-11.0	5.3	6.8	7.4	5.5	9.9	18.4	5.3	15.1	16.5
All	233	0.1	2.9	-10.9	5.7	7.2	7.9	5.8	10.1	18.8	6.9	15.9	18.0

Table 2.1: Error statistics for various multipath fading models in terms of terrain-climatic grouping of the links.

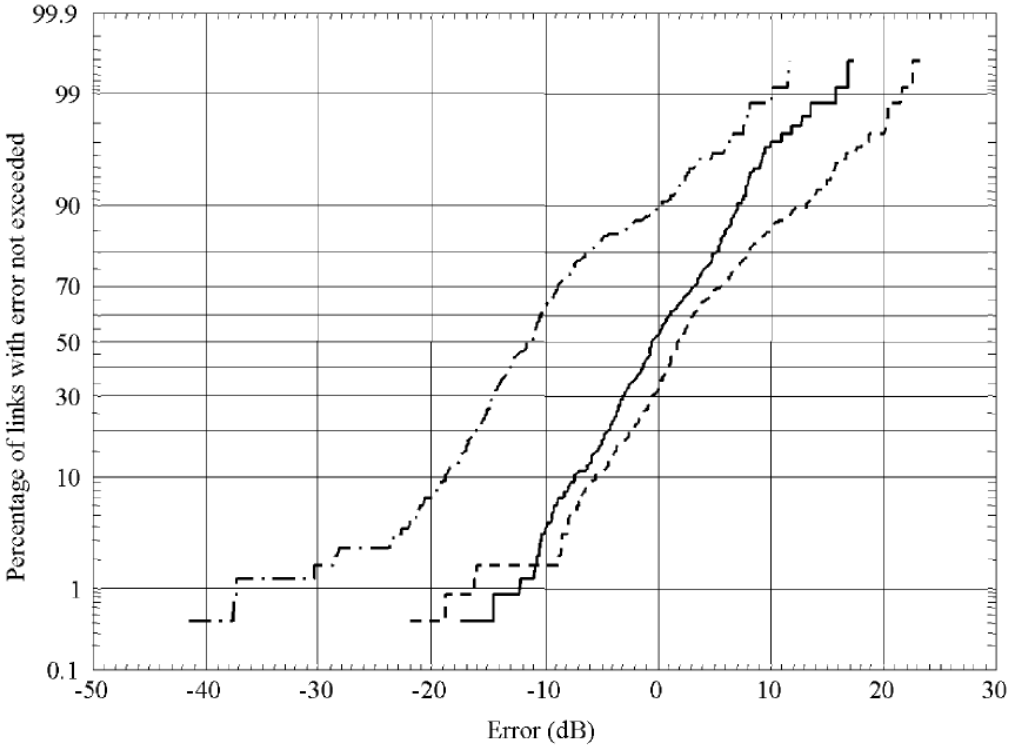

Figure 2.5: Cumulative distributions of error for the 239 links (including overland and overwater links) ITU-R P. 530-8 model (——); Barnett-Vigants model(- - -); Morita model(–. –. –.).

	ITU-R Model	**Barnett-Vigants Model**	**Morita Model**
-5 dB to 5 dB	60	59	16
-10 dB to 10 dB	93	83	36

Table 2.2: Percentage of links with error not exceeded in certain ranges.

According to Table. 2.1, ITU-R P.530 deep-fading distribution model has the best mean error performance overall and for most terrain-climatic groupings. On the other hand, the US (Barnett-Vigants) model overpredicts on average by 3.1 dB for all overland links, and the Japanese (Morita) model underpredicts on average by 11 dB. So, Olsen-Tjelta [5] paper said that the US model was developed for a range of latitudes below the average in the ITU-R database, and Japanase model was developed for a very mountainous country.

In Fig. 2.5, we have observed that 90 percentage of 239 links in Morita model, which predicted fade depth is smaller than measured fade depth with respect to 0 dB error criteria. 35 and 53 percent of 239 links in Barnett-Vigants model and

Rec. ITU-R P.530 model, which predicted fade depth is smaller than measured fade depth with regards to 0 dB error criteria, respectively.

As depicted in Table 2.2, the prediction values of Rec. ITU-R P.530 model are compatible with the measured values compared with the other multipath fading models. So, Rec. ITU-R P.530 model gives the best overall performance in modeling flat-fading statistics.

2.3 Case Studies for Multipath Fading Models

In this section, we have made case study simulation to compare results of three multipath fading outage models over sample terrestrial microwave LOS radio link located in Istanbul, Turkey. Fig. 2.6 shows the terrain path profile of Fenertepe-Sazlıtepe microwave radio LOS link. Terrain and climate parameters for Fenertepe-Sazlıtepe microwave LOS radio link are summarized in Table 2.3. We have analyzed the worst month link unavailability as a function of the fade margin with two different frequencies in NATO Band 3+ and 4 frequency ranges.

Comparison of derived parameters for three multipath fading outage models on Fenertepe-Sazlıtepe propagation path is shown in Table 2.4. The three models led to significantly different results for the link unavailability based on the fade margin, frequency, link path length and geoclimatic factor parameters. At the fixed link unavailability (p_w= 10^{-3}), fade margin can change up to 9.63 dB as shown in Fig. 2.7 and 2.8. The fade margin difference between Rec. ITU-R P.530 and Barnett-Vigants models increases with the frequency while its variaton between Morita and Rec. ITU-R P.530 models is slow with the frequency. Rec. ITU-R P.530 model has more climate and terrain parameters to design more accurate fixed terrestrial microwave radio LOS/NLOS links. So, there is a flexibility K factor value due to dN_1 and S_a parameters in contrast to Q and C propagation conditions factor values which are solely based on generic tables. It can be seen that Rec. ITU-R P.530 multipath fading mode is optimistic.

Parameter	Description
Transmitter station, Fenertepe	41^o N $09^{'}$ $2.40^{"}$ 28^o E $47^{'}$ $9.60^{"}$
Receiver station, Sazlıtepe	41^o N $08^{'}$ $43.40^{"}$ 28^o E $25^{'}$ $43.80^{"}$
Altitude of transmitter station (a.s.l)	220 m
Altitude of receiver station (a.s.l)	322 m
TX&RX antenna heights (a.g.l)	20 m
Radio frequency	1.350 and 5 GHz
Transmitted power	25 dBm
TX&RX antenna gains	27.15 dBi
Bandwith	20 MHz
Target SNR (64QAM5/6)	17.5 dB

Table 2.3: Terrestrial link parameters for Fenertepe-Sazlıtepe propagation path.

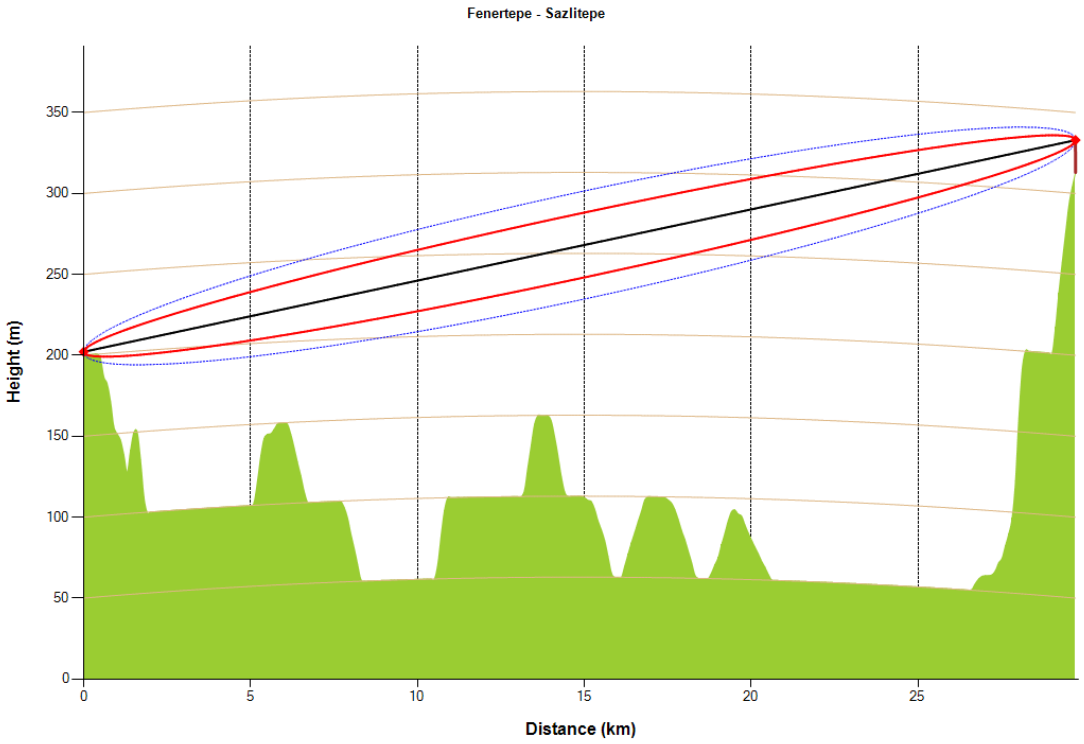

Figure 2.6: Terrain path profile of Fenertepe-Sazlıtepe microwave LOS radio link (the blue curve and the red curve indicate the first Fresnel zone and the 0.6 First Fresnel zone, respectively).

Parameter	Description
Path length	29.813 km
Path inclination	3.442 mrad
dN_1 for Rec. ITU-R P.530 model	-456.51 N-units/km
S_a for Rec. ITU-R P.530 model	100.7 m
Geoclimatic factor for Rec. ITU-R P.530 model	7.81×10^{-5}
Propagation conditions factor for Barnett-Vigants model	2
Average path height for Morita model	96.09 m
Propagation geoclimatic factor for Morita model	1.182×10^{-7}

Table 2.4: Comparison of derived parameters for three multipath fading models on Fenertepe-Sazlıtepe microwave LOS radio link

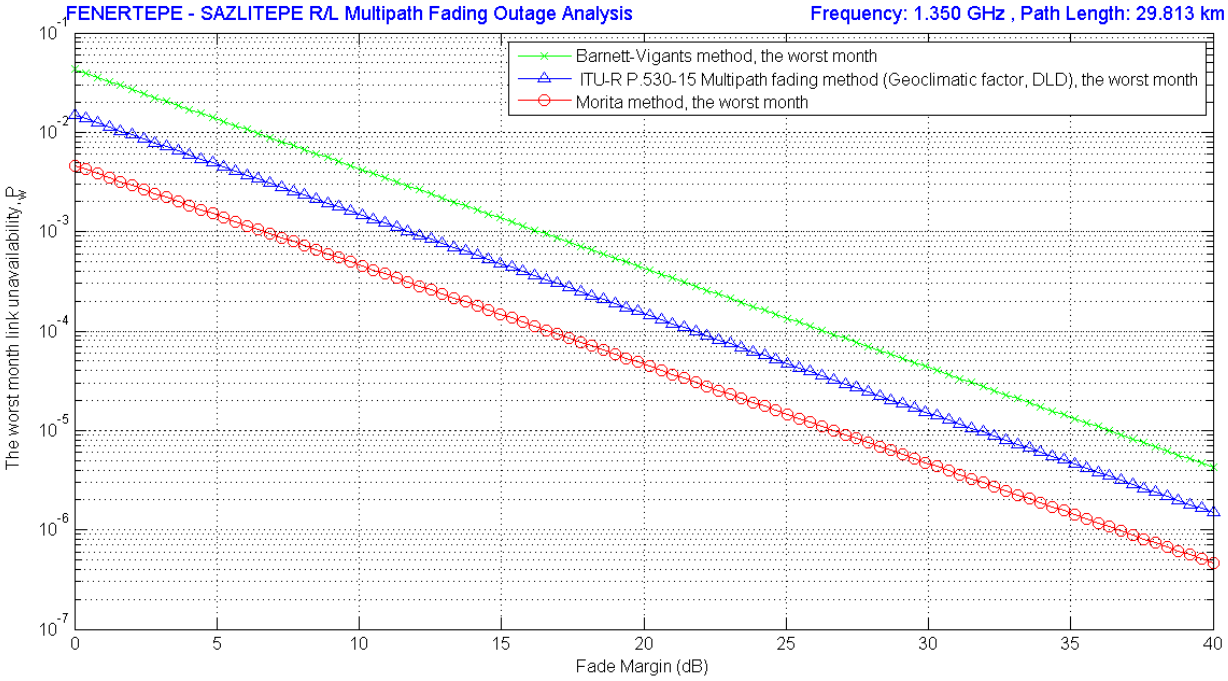

Figure 2.7: Percentage of time that fade depth has exceeded in the worst month for various multipath fading models, 1.350 GHz.

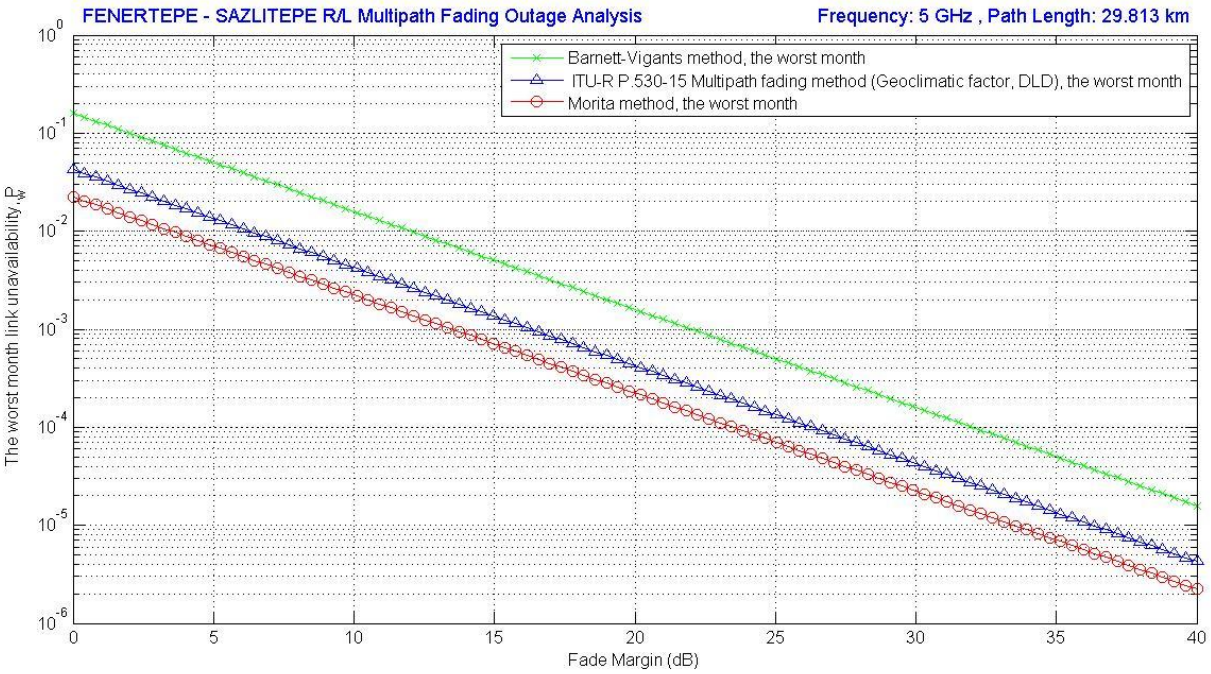

Figure 2.8: Percentage of time that fade depth has exceeded in the worst month for various multipath fading models, 5 GHz.

Chapter 3

PROPAGATION MECHANISMS ON TERRESTRIAL MICROWAVE RADIO LINK

Rec. ITU-R P.530 path loss prediction model [7] is composed of four significant clear-air and rainfall propagation mechanisms on the fixed terrestrial microwave LOS/NLOS radio links: attenuation due to atmospheric gases and rain, fading due to the multipath effects, and diffraction loss over terrain obstructions. This chapter focuses on the characteristics of the propagation mechanisms in clear-air and precipitation environments for terrestrial microwave LOS/NLOS radio links.

Table 3.1 summarizes Rec. ITU-R P.530 [7] and Rec. ITU-R P.526 [19] models referring to path propagation on the fixed terrestrial point-to-point sytems. Different propagation mechnanisms are an important constraint on the prediction of the path loss for terrestrial microwave LOS/NLOS radio links at different frequencies. For frequencies below 5 GHz, attenuation due to atmospheric gases and rain are small, and thus often neglected.

RECOMMENDATION ITU-R P.530 and P.526	
Application	Fixed Terrestrial Microwave LOS/NLOS Radio Link
Type	Point-to-Point Communication
Input	TX&RX Station Coordinates, TX&RX Antenna Heights (m, a.g.l), TX&RX Antenna Gains (dBi), TX Power (dBm), Path Length (km), Frequency (GHz), Percentage Time for Rain Attenuation (%), Polarization, SNR (dB), Bandwith (MHz), HPBW, Terrain Elevation Data, Climate Data.
Frequency	450 MHz-45 GHz
% time	All percentage of time in clear-air conditions, 0.001-1 in precipitation conditions.
Output	dN_1, Radio Refractivity Gradient (N-units/km), S_a, Terrain Roughness (m), Rain Rate (mm/h), Free Space Loss (dB), Path Loss (dB), Total Received Power (dBm), Noise Power (dBm), Fade Margin (dB), Link Availability (%).

Table 3.1: Path propagation parameters used in Rec. ITU-R P.530 and P.526.

3.1 Atmospheric Effects on Propagation

In radio transmission, attenuation occurs due to two mechanisms: absorption by atmospheric gases and rain. The attenuation due to absorption by atmospheric gases is explicitly listed as an effect to be included in the link budget. However, Rec. ITU-R P.530 does state: "On long paths at frequencies above about 20 GHz, it may be desirable to take into account known statistics of water vapour density and temperature in the vicinity of the defined path". This statement suggests that temporal variation of absorption fade may be significant at these higher frequencies and on long paths. Moreover, attenuation due to rain is much more significant at higher frequencies, especially above about 5 GHz.

3.1.1 Attenuation due to Atmospheric Gases

The transmission attenuation caused by atmospheric gases results from the molecular resonance of oxygen and water vapour. An oxygen molecule has a single permanent magnetic moment. At certain frequencies, its coupling with the magnetic field of an incident electromagnetic wave brings about resonance absorption. So, the principal cause of signal attenuation due to atmospheric gases is molecular absorption. Absorption by atmospheric gases depends on altitude above sea level, frequency, temperature, pressure and water vapour concentration. Rec. ITU-R P.676 [20] provides a method of calculating the specific attenuation with regards to meteorological informations provided by Study Group 3. Fig. 3.1 shows that specific attenuation from 1 to 350 GHz at sea-level for dry-air and water vapour with density of 7.5 g/m^3. At frequencies below 10 GHz, the excess attenuation due to atmospheric gases is slightly under 0.01 dB/km so that the attenuation due to atmospheric gases is insignificant in NATO Band 3+ and 4 frequency bands. However, absorption becomes serious contributors to path loss above 10 GHz.

For longer paths, the attenuation due to atmospheric gases should be taken into consideration in the calculation of the received signal power because the attenuation is directly proportional to the length of the path. The atmospheric attenuation on a path of length, d is given by [20, 21]:

$$A_{gas} = \gamma_{total} d = (\gamma_o + \gamma_w) d \quad (dB) \tag{3.1}$$

where γ_o and γ_w are the specific attenuation due to oxygen and water vapour in dB/km, respectively. In addition, γ_{total} is the total specific attenuation due to atmospheric gases in dB/km.

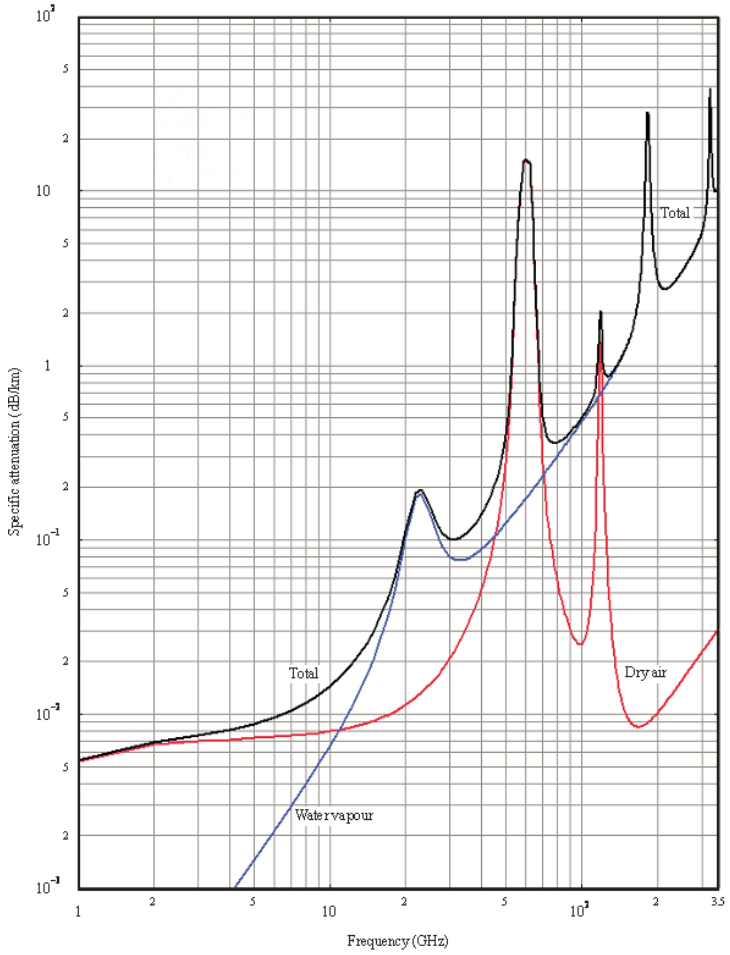

Figure 3.1: Specific attenuation due to atmospheric gases: atmospheric pressure, 1013 hPa; temperature, 15^o C; water vapour, 7.5 g/m^3.

3.1.2 Attenuation due to Rain

Attenuation due to rain is negligible at frequencies below 5 GHz. However, above 10 GHz, losses due to rain can cause outages, and it limits the availability of the terrestrial microwave LOS/NLOS radio link. Rain attenuation prediction procedure is shown in Fig. 3.2, and the rain attenuation is calculated in three stages.

The first stage, which estimates the rainfall rate at availability for 0.01%, requires the knowledge of rain rate distributions which characterize the geographical location of the defined microwave LOS/NLOS radio link. The rainfall rate exceeded for 0.01% of the time, $R_{001\%}$ (mm/h) is computed by using the procedure described in Rec. ITU-R P.837 [22].

In the second stage, specific attenuation due to rain in decibels per kilometer depends on various parameters including rainfall rate, polarization and frequency. The specific attenuation due to rain, γ_R (dB/km) is provided by Rec. ITU-R P.838 [23], and obtained from the rainfall rate, $R_{001\%}$ using the power law relationship:

$$\gamma_R = kR_{0.01\%}^{\alpha} \tag{3.2}$$

where k and α are frequency and polarization dependent coefficients. The coefficients can be determined using the following equations [23]:

$$log_{10}k_{h|v} = \sum_{j=1}^{4} a_j e^{-(\frac{\log_{10} f - b_j}{c_j})^2} + m_k \log_{10} f + c_k \tag{3.3}$$

$$\alpha_{h|v} = \sum_{j=1}^{5} a_j e^{-(\frac{\log_{10} f - b_j}{c_j})^2} + m_\alpha \log_{10} f + c_\alpha \tag{3.4}$$

Values for the constants required to calculate $k_{h|v}$ and $\alpha_{h|v}$ are provided by Rec. ITU-R P.838 [23]. The specific rain attenuation coefficient in Eq. (3.2) is calculated from the values by Eqs. (3.3) and (3.4) using the following equations:

$$k = [k_h + k_v + (k_h - k_v)cos^2(\theta)cos(2\tau)]/2 \tag{3.5}$$

$$\alpha = [k_h\alpha_h + k_v\alpha_v + (k_h\alpha_h - k_v\alpha_v)cos^2(\theta)cos(2\tau)]/2k \tag{3.6}$$

where θ is the path inclination and τ is the polarization tilt angle relative to the horizontal.

At the last stage, an effective path length is estimated to account for the rain inhomogeneous characteristic in the horizontal. The effective path length, $d_{eff} = r \times d$ using the folowing equation [7]:

$$r = \frac{1}{0.477d^{0.633}R_{0.01\%}^{0.073\times\alpha}f^{0.123} - 10.579(1 - e^{-0.024d}))} \tag{3.7}$$

where d is the actual length of a radio link in km and r is the path reduction factor.

Finally, multiplying the effective path length by the specific attenuation is equal to the rain attenuation at 0.01% exceeded level, $A_{0.01}$ (dB) is given by [7]:

$$A_{0.01} = \gamma_R d_{eff} \tag{3.8}$$

The attenuation exceeded for other percentages of time p in the range 0.001% to 1% may be deduced from the following power law:

$$A_p = A_{0.01} C_1 p^{-(C_2 + C_3 log_{10}(p))} \tag{3.9}$$

with:

$$C_1 = (0.07^{C_0}).(0.12^{1-C_0}) \tag{3.10}$$

$$C_2 = 0.855C_0 + 0.546(1 - C_0) \tag{3.11}$$

$$C_3 = 0.139C_0 + 0.043(1 - C_0) \tag{3.12}$$

where

$$C_0 = \begin{cases} 0.12 + 0.4[log_{10}(f/10)^{0.8})] & f \geq 10GHz \\ 0.12 & f < 10GHz \end{cases} \tag{3.13}$$

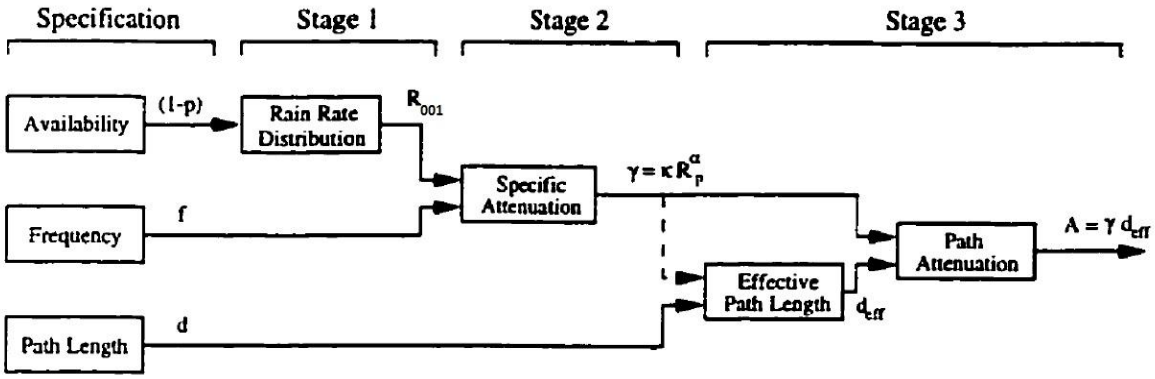

Figure 3.2: Rain attenuation prediction procedure.

The specific attenuation due to rain is given in the following figures for Ankara and Istanbul, Turkey. In Fig. 3.3 and 3.4, the specific attenuation due to rain are given as a function of the

- frequency (1-5 GHz)
- polarization (vertical and horizontal)
- p, the threshold that determines the rain rate which is exceeded p% of the time. In the figures, p= $1e^{-4}$ and p= $1e^{-3}$ are used, which corresponds to the link availability of 99.99% and 99.9%, respectively.

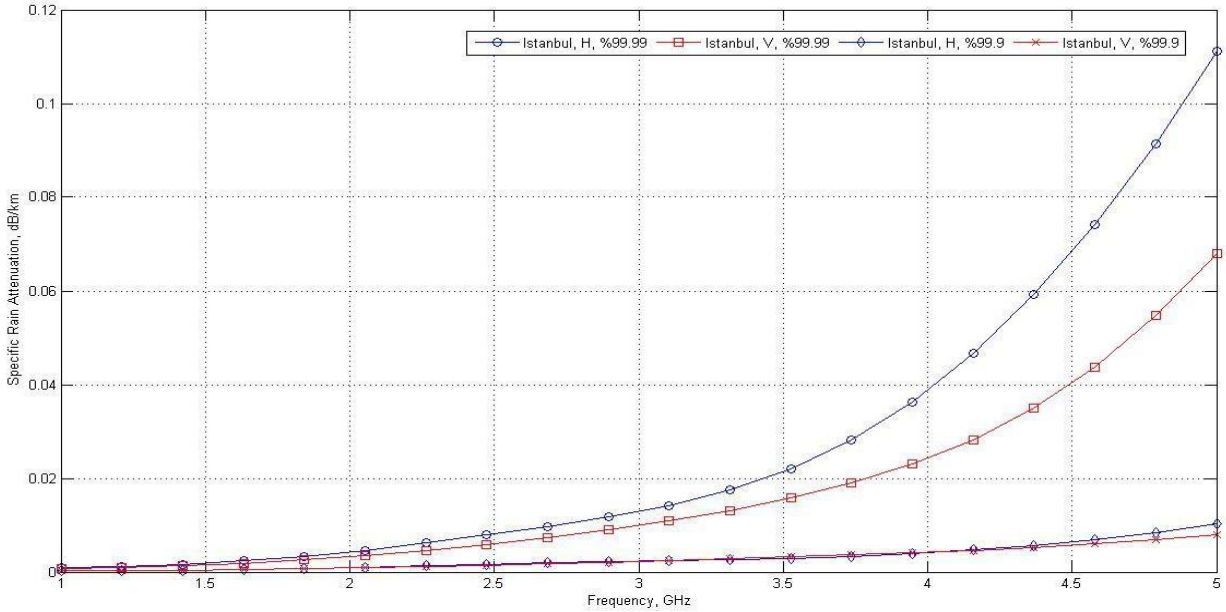

Figure 3.3: Specific attenuation due to rain for Sarıyer-Maslak radio link.

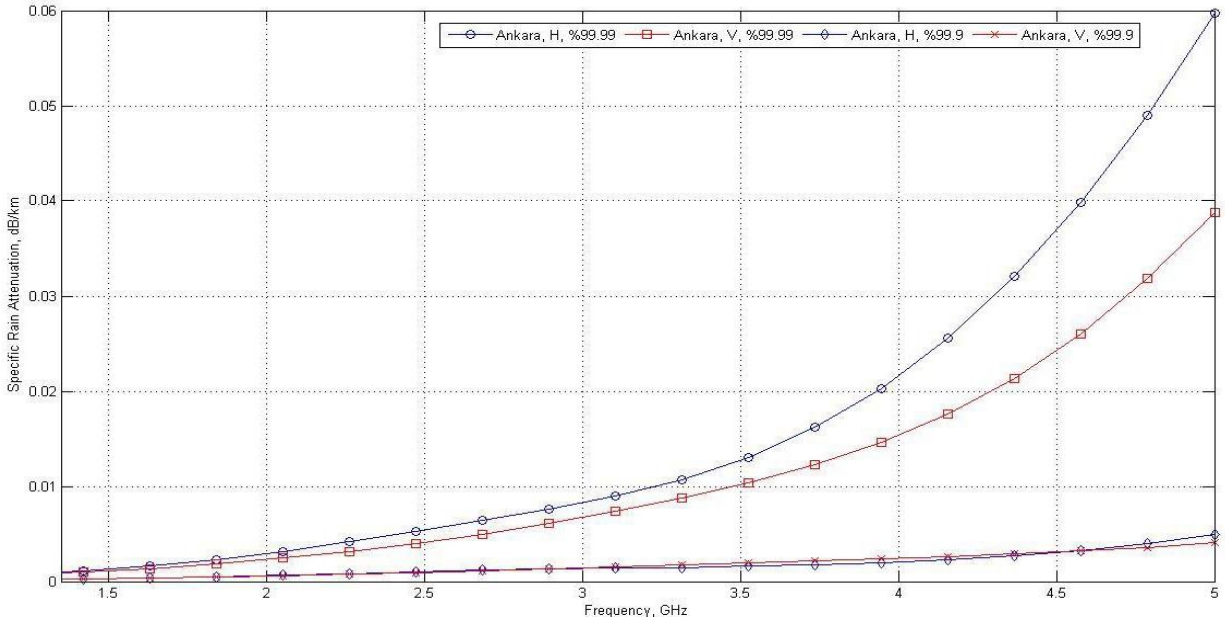

Figure 3.4: Specific attenuation due to rain for Polatlı-Elmadag radio link.

From Fig. 3.3 and 3.4, we make the following observations:

- The specific attenuation due to rain is negligible at frequencies below 5 GHz. However, the attenuation due to rain rapidly increases with frequency.
- The specific attenuation due to rain is considerably higher with horizontal polarization compared with vertical polarization.
- Attenuation due to rain depends on rain rate with respect to the location. i.e. the worst case of the path attenuation due to rain causes at 5 GHz, p= 0.01% (corresponding to a link availability of 99.99%), and horizontal polarization for Sarıyer-Maslak microwave LOS radio link.

The path attenuation due to rain as a function of path length varying between 1 and 50 km for the terrestrial microwave radio links are shown in the following figures. These plots are obtained for the highest frequency, i.e., the worst case, at 5 GHz and p= 0.01%, which corresponds to a link availability of 99.99%.

In Fig. 3.5 and 3.6, we have observed that the attenuation due to rain as a function of both vertical polarization and a 50 km path ranges from 0.75 dB at Ankara to nearly 1.1 dB at Istanbul. On the other hand, the attenuation due to rain in horizontal polarization tended to be slightly larger than that in vertical polarization for longer path at Istanbul, Turkey.

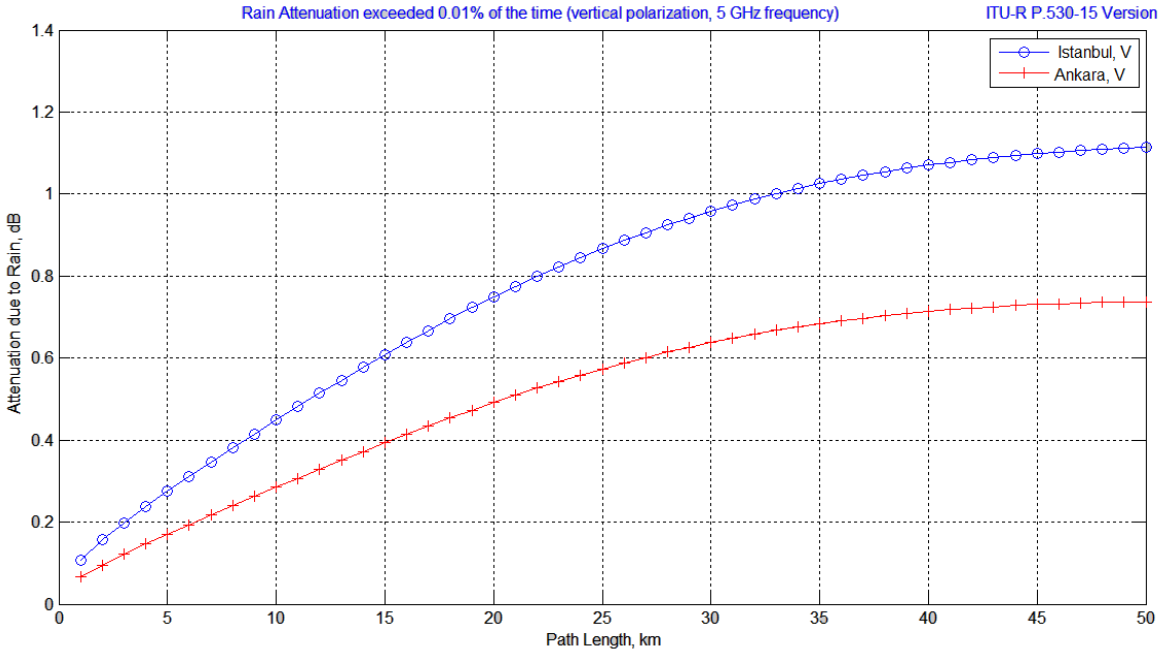

Figure 3.5: Rain attenuation on terrestrial 5 GHz link as a function of vertical polarization.

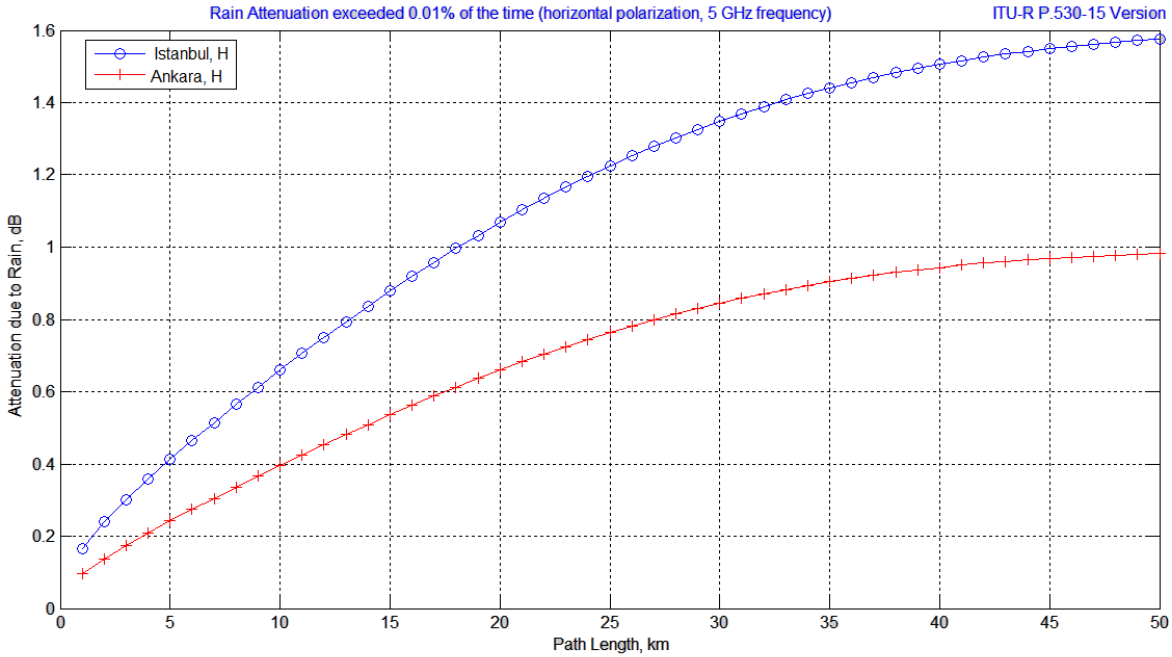

Figure 3.6: Rain attenuation on terrestrial 5 GHz link as a function of horizontal polarization.

3.2 Diffraction Fading

Diffraction phenomenon occurs when 60% of the first Fresnel zone is obstructed by an obstacle or several obstacles between the transmitter and receiver sites. To make the calculation of the diffraction loss, it is necessary to identify the form of the obstacles assuming a knife-edge of negligible thickness. Diffraction loss depends on the heights of hilltops with respect to the heights of the transmitter and receiver sites taking into account the effective Earth radius related to ray-path bending in the atmosphere, and the horizontal distances of the terrain path profile points from the transmitter site.

Diffraction fading is based on the Huygen's principle where each point of a wavefront represents an infinite secondary source of a new spherical wave [24]. The wavelets above the obstacle propagation to all directions include the shadowed area behind the obstacle. An illustration of shadowing of radio waves by an object is found in Fig. 3.7.

3.2.1 Single Knife-Edge Diffraction Model

If the direct line-of-sight path is obstructed by a single knife-edge type of obstacle as illustrated in Fig. 3.8, height of the top of the obstacle above the straight line joining the two ends of the path, h. The knife-edge diffraction parameter is defined as [19]:

$$v = h\sqrt{\frac{2(d_1 + d_2)}{\lambda d_1 d_2}} \tag{3.14}$$

$$v = \theta\sqrt{\frac{2d_1 d_2}{\lambda(d_1 + d_2)}} \tag{3.15}$$

$$v = \sqrt{\frac{2d\alpha_1\alpha_2}{\lambda}} \tag{3.16}$$

where d_1 and d_2 are the terminal slant distances from the knife-edge obstacle in km, θ is angle of diffraction in radians, α_1 and α_2 are angles in radians between the top of the obstacle and one end as seen from the other end. α_1 and α_2 are of the sign of h in the above equations. Hence, the phase difference is written as [19]:

$$\phi = \frac{\pi v^2}{2} \tag{3.17}$$

Therefore, the total sum of contributions up to v as the complex Fresnel integral is written as [19]:

$$F(v) = \int_0^v e^{j\frac{\pi t^2}{2}} dt = C(v) + jS(v) \tag{3.18}$$

where

$$C(v) = \int_0^v cos(\frac{\pi t^2}{2})dt, \quad S(v) = \int_0^v sin(\frac{\pi t^2}{2})dt \tag{3.19}$$

The electric field strength, E_k, of a knife-edge diffracted wave is given by:

$$E_k = \int_v^\infty e^{j\frac{\pi t^2}{2}} dt \tag{3.20}$$

Assuming that the value of the Cornu spiral for infinity is $0.5 + j0.5$. The field strength, E_k is then expressed using the finite integral:

$$E_k = (0.5 + j0.5) - \int_0^v e^{j\frac{\pi t^2}{2}} dt = [0.5 - C(v)] + j\,[0.5 - S(v)] \tag{3.21}$$

The electric field strength relative to free space is given by [19]:

$$E_{field} = \frac{E_k}{E_o} = \frac{\sqrt{[1 + C(v) - S(v)]^2 + [C(v) - S(v)]^2}}{2} \tag{3.22}$$

For the purposes of simplification in Rec. ITU-R P.526 [19], the diffraction loss is calculated by the following formula:

$$A_{diff}(dB) = \begin{cases} 6.9 + 20log(\sqrt{(v-0.1)^2+1} + v - 0.1) & v > -0.78 \\ -20log(E_{field}) & others \end{cases} \tag{3.23}$$

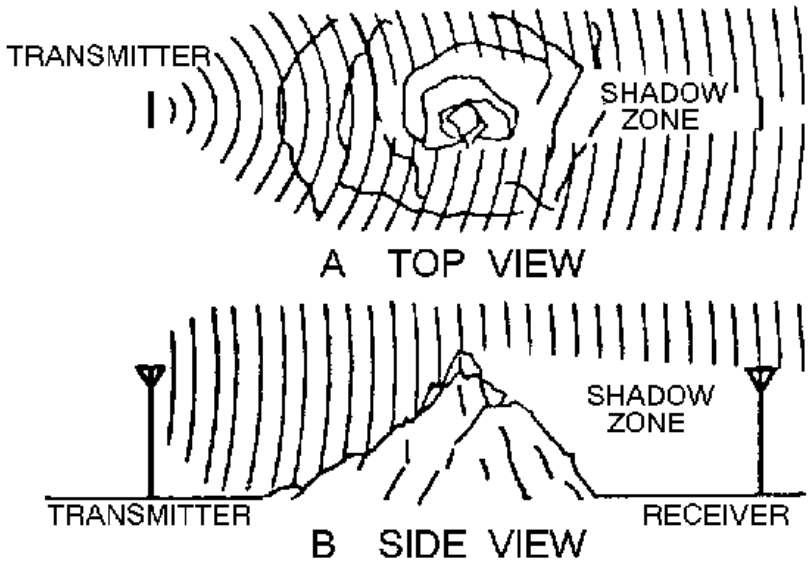

Figure 3.7: Shadowing of radio waves by an object.

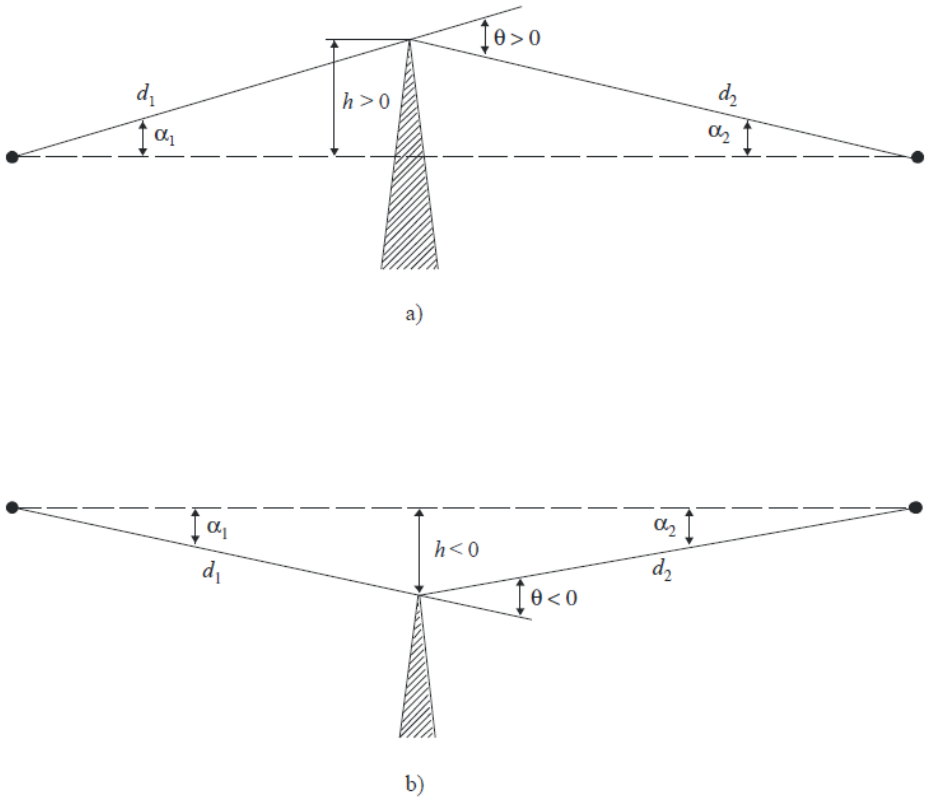

Figure 3.8: Illustration of different single knife-edge diffraction scenarios. (a) NLOS path case and α_1, α_2 and v are positive, since h is positive (b) LOS path case and α_1, α_2 and v are negative, since h is negative.

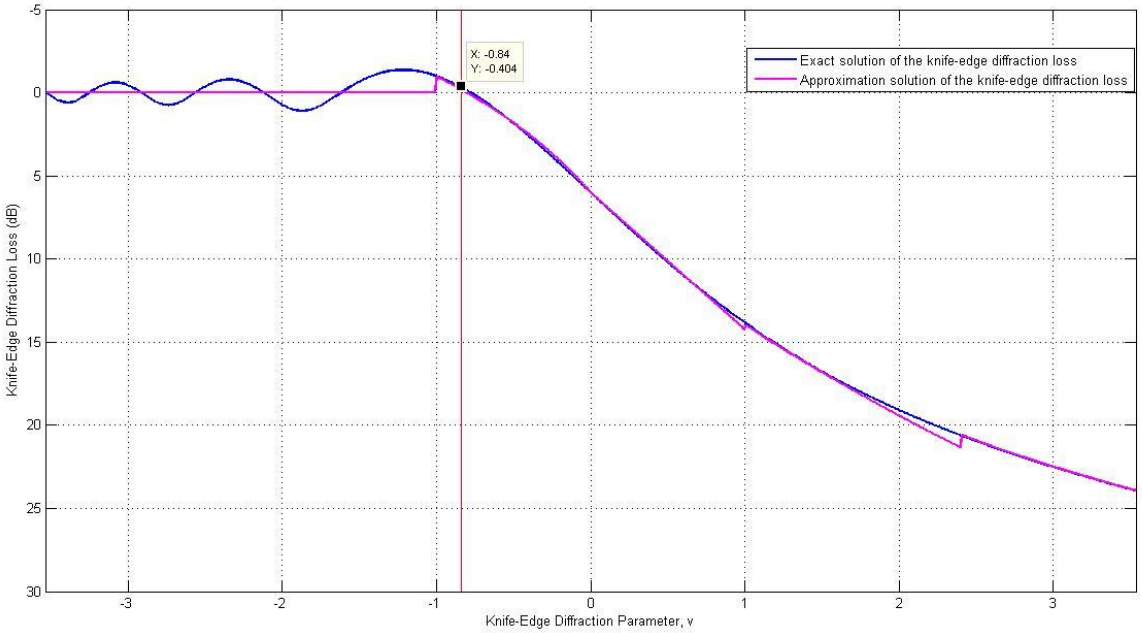

Figure 3.9: Knife-edge diffraction loss as a function of Fresnel knife-edge diffraction parameter.

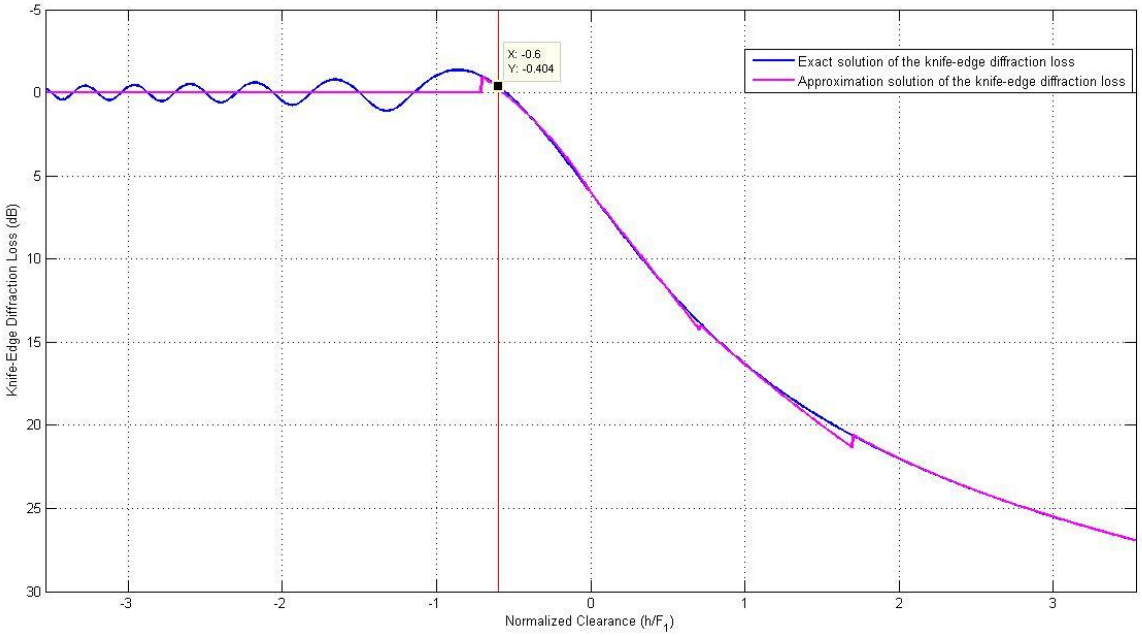

Figure 3.10: Knife-edge diffraction loss as a function of normalized clearance.

In addition, an approximate solution for Eq. (3.23) provided by Lee [25] is given by the following formula:

$$Loss(dB) = \begin{cases} 0 & v \leq -1 \\ 20log(0.5 - 0.62v) & -1 \leq v \leqslant 0 \\ 20log(0.5e^{-0.95v}) & 0 \leq v \leqslant 1 \\ 20log(0.4 - \sqrt{0.1184 - (0.38 - 0.1v)^2}) & 1 \leq v \leqslant 2.4 \\ 20log(\frac{0.255}{v}) & v > 2.4 \end{cases} \tag{3.24}$$

In Fig. 3.9 and 3.10, comparison of an exact and approximation solution for the diffraction loss due to the presence of a single knife-edge are made. If Fresnel knife-edge diffraction parameter is smaller than -0.84 or clearance is smaller than -0.6F_1, the appearing blockage between transmitter and receiver sites can be insignificant on the Fresnel ellipsoid zone. So, the direct path between transmitter and receiver sites needs a clearance above ground of at least 60% of the radius of the first Fresnel zone to ignore the effect of the diffraction loss.

3.2.2 Double Knife-Edge Diffraction Model

In many practical situations, especially in hilly terrain environment, the propagation path consists of more than one obstruction in which case the diffraction loss due to all of the obstacles must be computed. These effects are generally estimated using: (i) the classical prediction models proposed by Bullington, Deygout and Epstein-Peterson [26–28], with modifications; (ii) the ones described by the most recent versions of Recommendations ITU-R P.526 [19]. In that case of two obstacles, the diffraction loss is calculated over the LOS line (trans-horizon path type) whereby using the different prediction methods: (i) Deygout, (ii) Epstein-Peterson and (iii) Delta-Bullington. The primary limitation of Deygout and Epstein-Peterson diffraction methods is that correction terms are not defined for the multiple knife-edge case mentioned in Rec. ITU-R P.526. So, these diffraction prediction methods are only used for two obstacles over the LOS line.

3.2.2.1 Deygout Method

This method consists of applying single knife-edge diffraction theory successively to the two obstacles along the terrestrial microwave NLOS radio link. The first step in the Deygout method is choosing a dominant edge, which is the obstacle with the highest Fresnel diffraction parameter. The main diffraction loss caused only by the dominant obstacle and is then summed with the loss from other obstacle whose height is given by the line between the transmitter or receiver site and the top of the dominant edge. Fig 3.11 shows the construction for an approximate calculation of the double knife-edge diffraction loss proposed by Deygout [19].

In Fig. 3.11, the first edge is predominant and the first diffraction path is defined by the distances a and $b + c$, and the clearance h_1, gives a diffraction loss L_1 (dB). The second diffraction path is defined by the distances b and c, and the clearance $h_2^{'}$, gives a loss L_2 (dB). L_1 and L_2 are calculated by using formula of Eq. (3.23).

A diffraction correction term, *Correction(dB)* [19], is calculated by using Eq. (3.25), and then must be subtracted over the total diffraction loss to take into account the separation between the two edges as well as their height.

$$Correction = [12 - 20log(\frac{2}{1 - \frac{a}{\pi}})](\frac{q}{p})^{2p} \ \ (dB) \tag{3.25}$$

where

$$p = [\frac{2}{\lambda}\frac{d}{(b+c)a}]^{0.5} h_1 \tag{3.26}$$

$$q = [\frac{2}{\lambda}\frac{d}{(a+b)c}]^{0.5} h_2 \tag{3.27}$$

$$\alpha = \arctan(\frac{bd}{ac})^{0.5} \tag{3.28}$$

$$d = a + b + c \ \ (km) \tag{3.29}$$

Finally, the total diffraction loss is calculated as [19]:

$$L = L_1 + L_2 - Correction \ \ (dB) \tag{3.30}$$

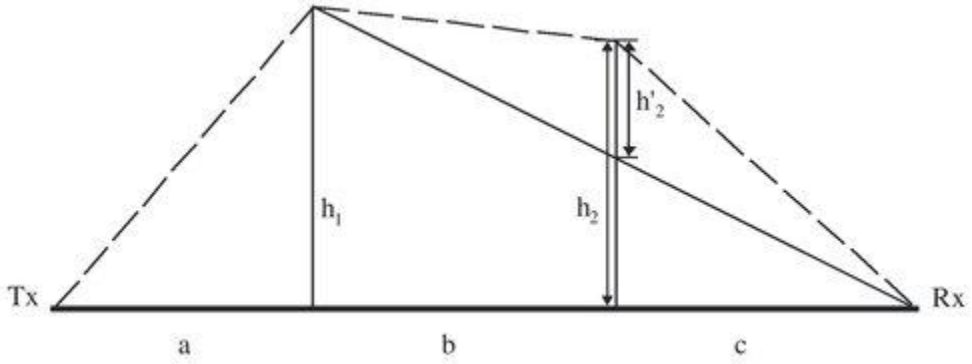

Figure 3.11: Deygout method geometry over the LOS line.

3.2.2.2 Epstein-Peterson Method

In this method, a propagation path is divided into three subpaths, each of which has one knife-edge diffraction loss, and their power sum gives the total diffraction loss caused by knife-edge of negligible thickness. The sub-path is given by the single knife-edge obstacle whose height is computed from the connection between two adjacent obstacles.

As shown in Fig. 3.12, the first diffraction path is defined by the distances a and b, and the clearance $h_1^{'}$, gives a diffraction loss L_1 (dB). The second diffraction path is also defined by the distances b and c, and the clearance $h_2^{'}$, gives a diffraction loss L_2 (dB). L_1 and L_2 are calculated by using formula of Eq. (3.23). A diffraction correction term, *Correction(dB)* [19], must be added to take into account the separation b distance between the edges.

$$Correction = \begin{cases} 10log(\frac{(a+b)(b+c)}{bd}) & L_1 \; or \; L_2 \geq 15dB \\ 0 & others \end{cases} \tag{3.31}$$

where

$$d = a + b + c \;\; (km) \tag{3.32}$$

Finally, the total diffraction loss is calculated as [19]:

$$L = L_1 + L_2 + Correction \;\; (dB) \tag{3.33}$$

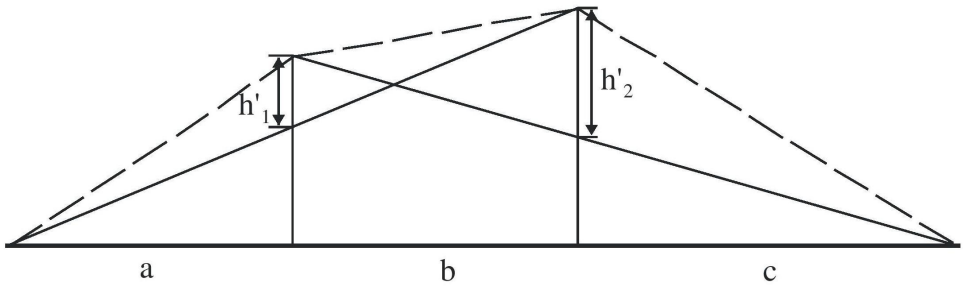

Figure 3.12: Epstein-Peterson method geometry over the LOS line.

3.2.3 Multiple Knife-Edge Diffraction Model

If the propagation path consists of more than a single obstruction along the path profile, Rec. ITU-R P.526 model provides Epstein-Peterson, Deygout and Delta-Bullington methods to predict the total diffraction loss due to multiple knife-edges, but the Epstein-Peterson and Deygout diffraction prediction methods used only for two obstacles over the LOS line. In addition, if none of the knife-edges are above the LOS line, then Rec. ITU-R P.526 suggests only Delta-Bullington method on the calculation of the diffraction loss. For this case, Delta-Bullington method is not based on constructing an equivalent hypothetical single knife-edge at the intersection of transmitter and receiver sites because the actual terrain profile point with the highest Fresnel diffraction parameter is found along the terrain path profile. Alternatively, the modified Bullington model has been proposed for supporting the Bullington construction in LOS path case.

3.2.3.1 Delta-Bullington Method

Delta-Bullington method has three parts as shown below:

- 1. Actual terrain profile and antenna heights above sea level are used to calculate the Bullington diffraction loss, L_b(dB).
- 2. A smooth surface profile consists of the modified antenna heights at the transmitter and receiver sites, and setting all other profile point h_i to

zero. Bullington method is again applied for this smooth surface terrain profile to calculate the diffraction loss, L_{bs}(dB). So, the Bullington part of Delta-Bullington method is used twice.

- 3. The modified antenna heights of the smooth surface at the transmitter and receiver sites, electrical characteristics of the surface of the Earth, and equivalent Earth's radius are input to the spherical-Earth diffraction model. The predicted spherical-Earth diffraction loss is L_{sph}(dB).

In the following equations are related to the Bullington part of Delta-Bullington method. The distance and height of the i-th profile point are d_i (km) and h_i (m, above sea level) respectively, i takes values from *1* to n where n is the number of profile points. Transmitter and receiver heights are h_{tx} and h_{rx} (m, above sea level) respectively, and the complete path length is d (km). Effective Earth curvature C_e $(1/\ km)$ is given by $1/\ r_e$ where r_e is effective Earth radius in km.

This method replaces several obstacles over the LOS line by one single knife-edge obstacle whose height is given by the intersection of lines: the dominant clearance profile point from transmitter site to receiver site is shown in Fig 3.13.

Firstly, the dominant profile point with the highest slope of the line from the transmitter to the i-th profile point is given by [19]:

$$S_{tim} = max[\frac{h_i + 500C_e d(d - d_i) - h_{tx}}{d_i}] \ \ (mrad) \tag{3.34}$$

The slope of the LOS line from transmitter to receiver is calculated as [19]:

$$S_{tr} = \frac{h_{rx} - h_{tx}}{d} \ \ (mrad) \tag{3.35}$$

Two path cases are classsified as shown below:

$$Path\ Type = \begin{cases} LOS & S_{tim} \leqslant S_{tr} \\ Transhorizon & S_{tim} > S_{tr} \end{cases} \tag{3.36}$$

Case 1. Path Profile is LOS

This model is not based on constructing an equivalent hypothetical single knife-edge at the intersection of transmitter and receiver sites, but the profile point with the highest Fresnel diffraction parameter, v_{max} is found along the terrain path profile.

$$v_{max} = max[h_i + 500C_e d(d - d_i) - \frac{h_{tx}(d - d_i) + h_{rx}d_i)}{d}]\sqrt{\frac{0.002d}{\lambda d_i(d - d_i)}} \quad (3.37)$$

In this case, the excess loss of the profile point is calculated as [19]:

$$L_{knife}(dB) = \begin{cases} 6.9 + 20log(\sqrt{(v_{max} - 0.1)^2 + 1} + v_{max} - 0.1) & v_{max} > -0.78 \\ 0 & others \end{cases} \quad (3.38)$$

Case 2. Path Profile is Transhorizon

The dominant profile point with the highest slope of the line from the receiver to the i-th profile point is given by [19]:

$$S_{rim} = max[\frac{h_i + 500C_e d(d - d_i) - h_{rx}}{d - d_i}] \ \ (mrad) \quad (3.39)$$

One hypothetical knife-edge obstacle is defined by the intersection of S_{tim} and S_{rim}. The distance of an equivalent knife-edge obstacle from the transmitter site is given by [19]:

$$d_{eq} = \frac{h_{rx} - h_{tx} + S_{rim}d}{S_{tim} + S_{rim}} \ \ (mrad) \quad (3.40)$$

Calculation of the Fresnel diffraction parameter, v_{eq} for an equivalent knife-edge obstacle is given by [19]:

$$v_{eq} = [h_{tx} + S_{tim}d_{eq} - \frac{h_{tx}(d - d_{eq}) + h_{rx}d_b)}{d}]\sqrt{\frac{0.002d}{\lambda d_{eq}(d - d_{eq})}} \quad (3.41)$$

In this case, the excess loss of an equivalent knife-edge obstacle is calculated as:

$$L_{knife}(dB) = \begin{cases} 6.9 + 20log(\sqrt{(v_{eq} - 0.1)^2 + 1} + v_{eq} - 0.1) & v_{eq} > -0.78 \\ -20log(F) & others \end{cases} \quad (3.42)$$

where

$$F = \frac{\sqrt{[1 + C(v_{eq}) - S(v_{eq})]^2 + [C(v_{eq}) - S(v_{eq})]^2}}{2} \tag{3.43}$$

The diffraction loss is calculated by using either Eqs. (3.38) or (3.42), and Bullington diffraction loss with the correction term is given by [19]:

$$L_b = L_{knife} + [1 - e^{\frac{-L_{knife}}{6}}](10 + 0.02d) \ \ (dB) \tag{3.44}$$

The overall diffraction loss of the terrain path profile is calculated as [19]:

$$L = L_b + max(L_{sph} - L_{bs}, 0) \ \ (dB) \tag{3.45}$$

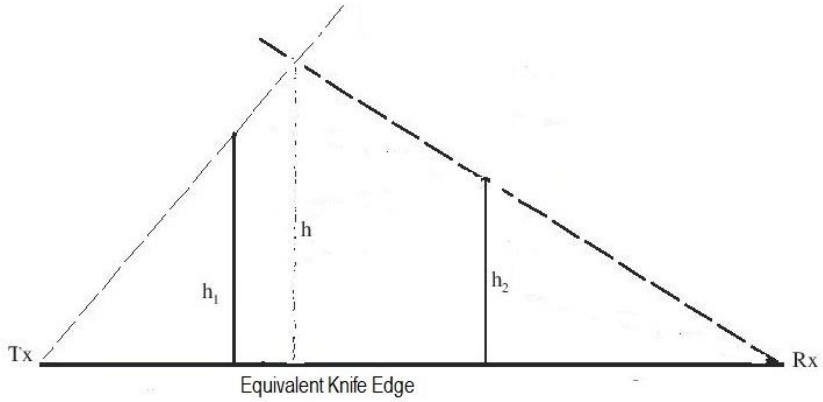

Figure 3.13: Bullington method geometry over the LOS line.

3.2.3.2 Proposed Diffraction Method

If the propagation path consists of more than one obstruction over the LOS line, the proposed method can give the same result with Delta-Bullington method, but we have proposed the diffraction method to apply the Bullington construction on the LOS path case.

In the following equations, effective curvature of the Earth is given by k factor, and Earth radius, R is 6371 km. The line-of-sight height of the i-th path profile point is $line_i$ (m), i takes values from *1* to n where n is the number of profile points. The clearance of i-th path profile point is given by:

$$clearance_i = h_i + Earth - line_i \ \ (m) \tag{3.46}$$

Firstly, the dominant profile point with the highest slope of the line from the transmitter site to the i-th path profile point is determined by using formula of Eq. (3.47), and the highest slope of the line from the receiver site to the i-th path profile point is found by using formula of Eq. (3.48).

$$S_{tim} = max[\frac{h_i + Earth - h_{tx}}{d_i}] \ \ (mrad) \tag{3.47}$$

$$S_{rim} = max[\frac{h_i + Earth - h_{rx}}{d - d_i}] \ \ (mrad) \tag{3.48}$$

where

$$Earth = 1000 \times kR[1 - \frac{cos(\frac{d}{2kR})}{cos\left|\frac{\frac{d}{2} - d_i}{kR}\right|}] \ \ (m) \tag{3.49}$$

One hypothetical knife-edge obstacle is defined by the intersection of S_{tim} and S_{rim}. The distance of an equivalent knife-edge obstacle from the transmitter site is calculated by using formula of Eq. (3.40). The clearance of an equivalent knife-edge obstacle is expressed as:

$$h_{clearance} = \sum_{i=1}^{j} \frac{1}{clearance_i} \tag{3.50}$$

where j is the number of obstacles along the terrain path profile.

Calculation of the Fresnel diffraction parameter, v_{eq} for an equivalent knife-edge obstacle is given by:

$$v_{eq} = h_{clearance}\sqrt{\frac{0.002d}{\lambda d_{eq}(d - d_{eq})}} \tag{3.51}$$

In that case, the diffraction loss of an equivalent knife-edge obstacle is calculated by using formula of Eq. (3.52). Then, Bullington diffraction loss with the correction term is calculated by using formula of Eq. (3.44).

$$L_{knife}(dB) = \begin{cases} 6.9 + 20log(\sqrt{(v_{eq} - 0.1)^2 + 1} + v_{eq} - 0.1) & v_{eq} > -0.78 \\ -20log(F) & others \end{cases} \tag{3.52}$$

3.3 Diffuse Reflection Loss

In this section, we have described the multipath fading caused by the reflection points on the terrestrial microwave line-of-sight radio link. The calculation method of reflection points on the terrain path profile is based on the two-ray ground reflection model, and the determination of reflection points along the terrain path profile is improved. The procedure for finding reflection points is to proceed along the path from transmitter site to receiver site, and each path profile point evaluates whether a specular reflection can exist in the profile point in which the angle of incident from the transmitter is equal to the angle of reflection to the receiver. The strength of the reflected signal at the receiving antenna depends on the specular reflection coefficient, the divergence factor due to Earth curvature, grazing angle, polarization and the directivity of the antennas.

The specular reflection coefficient of the surface, ρ is given by [7]:

$$\rho = \left| \frac{sin\phi - \sqrt{C}}{sin\phi + \sqrt{C}} \right| \tag{3.53}$$

where ϕ is the grazing angle and

$$C = \begin{cases} \eta - cos^2\phi & for\ horizontal\ polarization \\ (\eta - cos^2\phi)/\eta^2 & for\ vertical\ polarization \end{cases} \tag{3.54}$$

with

$$\eta = \varepsilon_r - j18\frac{\sigma}{f} \tag{3.55}$$

where ε_r is the relative permittivity and σ is the conductivity (S/m). In Fig. 3.14, the values of conductivity and permittivity for different types of ground as a function frequency are given in Rec. ITU-R P.527 [29].

When an electromagnetic wave is incident on a round path surface, the reflected wave diverges because of the path surface. So, the energy of the reflected signal is defocused due to divergence. The calculation of the divergence factor of the Earth's surface is mentioned in Rec. ITU-R P.530 [7].

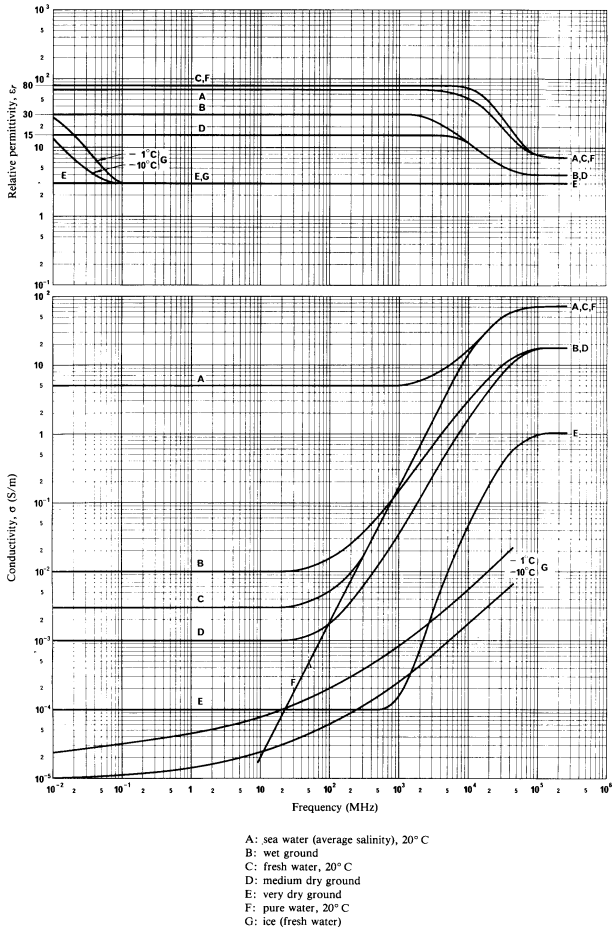

Figure 3.14: Relative permittivity, ε_r and conductivity, σ (S/m) as a function of frequency.

In addition to divergence factor, surface roughness property also affects the diffuse reflection coefficient. If the surface within the 1^{st} Fresnel ellipse is somewhat rough, the calculation of the surface roughness factor, ρ_s is also mentioned in Rec. ITU-R P.530 [7].

The diffuse or effective reflection coefficient is given by [7]:

$$\rho_{eff} = \rho D \rho_s \tag{3.56}$$

Calculation of the loss in the level of the surface reflected signals relative to the direct signal taken into account by antenna discrimination [7]:

$$L_a = 12[(\frac{\alpha_1}{\alpha_{HPBW_{TX}}})^2 + (\frac{\alpha_2}{\alpha_{HPBW_{RX}}})^2] \ \ (dB) \tag{3.57}$$

where α_1 and α_2 are the angles between the direct and reflected waves at transmitter and receiver sites, $\alpha_{HPBW_{TX}}$ and $\alpha_{HPBW_{RX}}$ are the half-power beamwidth of the antennas.

The overall loss due to surface reflected wave is given by [7]:

$$L_s = L_a - 20log(\rho_{eff}) \ \ (dB) \tag{3.58}$$

If the path profile consists of more than one reflection point on the terrestrial microwave LOS radio link, the reflection loss of the microwave LOS radio link can be taken as the minimum of the overall losses due to reflection points, $\min(L_s)$.

We have made case study simulation to examine the impact of both polarization and ground type on the calculation of the diffuse reflection loss. In Table 3.2, four possible reflection points are existed along the Fenertepe-Sazlıtepe microwave radio LOS link with 100 m distance increment. Third reflection point (13.691 km distance from Fenertepe site) has the minimum overall reflection loss when compared with the losses of the other reflection points on this link. The half-power beamwidth of the antenna is 8^o at 2 GHz frequency. The values of conductivity and permittivity for different types of ground are shown in Table 3.3.

According to Table 3.4 and 3.5, the diffuse reflection coefficient for vertical polarization is less than the coefficient for horizontal polarization on the same ground type. The values of ground reflection loss from Fresh Water to Medium Dry Ground type increase for vertical polarization, but reduce for horizontal polarization. These results are in concordance with the Report 1008-1 [30].

Possible Reflection Points (km)	**Grazing Angle (deg.)**	**Divergence Factor**
0.105	5.606	0.993
5.975	0.505	0.997
13.691	0.422	0.997
28.246	2.541	0.998

Table 3.2: Main parameters used for reflection case study.

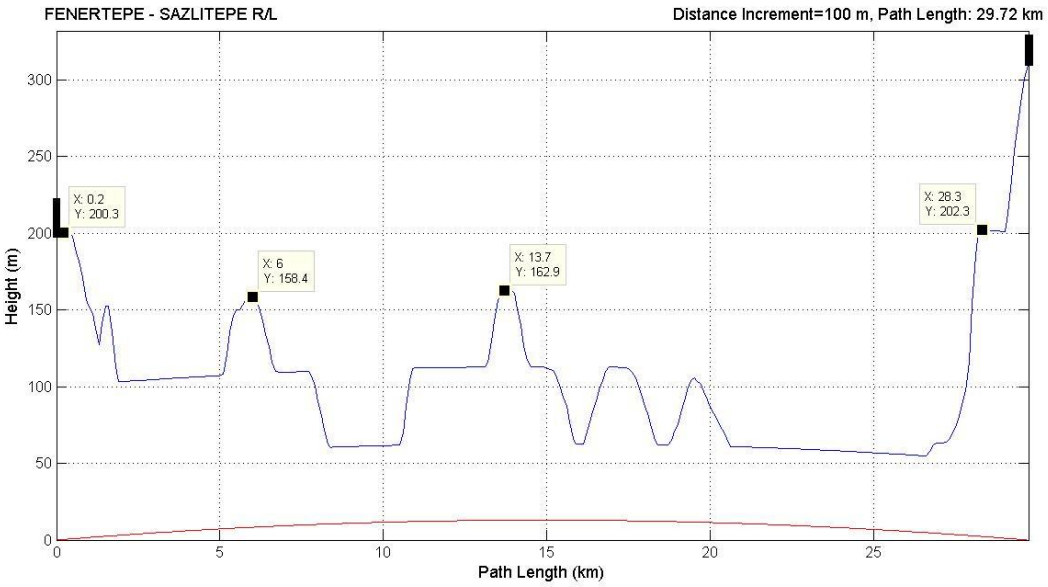

Figure 3.15: The geometry of the reflected propagation path.

Ground Type	**Relative Permittivity**	**Conductivity (S/m)**
Fresh Water	80	0.6
Sea Water	70	6.007
Wet Ground	30	0.4
Medium Dry Ground	15	0.116
Ice Water	3	0.0006

Table 3.3: The values of conductivity and relative permittivity for different types of ground at 2 GHz frequency.

Ground Type	**Diffuse Reflection Coeffiecient** ρ_{eff}	**Reflection Loss,** L_s **(dB)**
Fresh Water	0.874	1.22
Sea Water	0.875	1.21
Wet Ground	0.919	0.78
Medium Dry Ground	0.941	0.58
Ice Water	0.967	0.34

Table 3.4: Reflection case study results for different types of ground and vertical polarization on Fenertepe-Sazlıtepe microwave LOS link.

Ground Type	**Diffuse Reflection Coeffiecient** ρ_{eff}	**Reflection Loss,** L_s **(dB)**
Fresh Water	0.996	0.084
Sea Water	0.996	0.082
Wet Ground	0.995	0.093
Medium Dry Ground	0.994	0.103
Ice Water	0.987	0.34

Table 3.5: Reflection case study results for different types of ground and horizontal polarization on Fenertepe-Sazlıtepe microwave LOS link.

Chapter 4

LINK ANALYSIS AND SIMULATION STUDIES

The main propagation effects must be considered in the calculation of the link availability on the terrestrial microwave LOS/NLOS radio link as shown below:

- Free space loss,
- Attenuation due to atmospheric gases,
- Attenuation due to precipitation,
- Diffraction fading due to obstruction(s) of the path terrain profile,
- Multipath fading due to multipath arising from surface reflection points.

This chapter describes the link budget calculation process, and discusses the terrain path profile of the terrestrial microwave LOS/NLOS radio link. Examples of simulation studies are given at the end of this chapter. In a typical microwave radio link schematic is shown in Fig. 4.1.

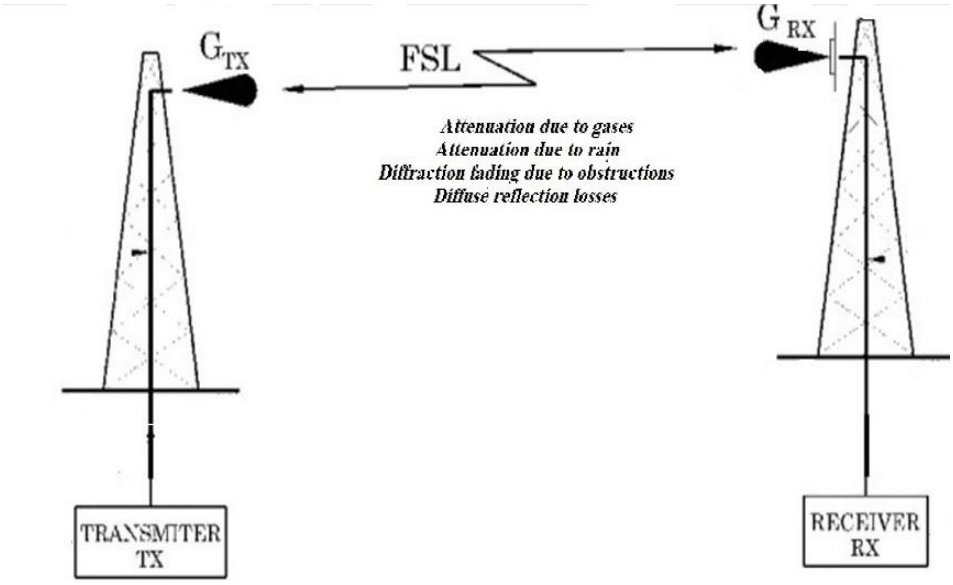

Figure 4.1: An illustration of a typical microwave radio link.

4.1 Link Power Budget

The prediction of the received signal power is a crucial in the design of fixed terrestrial microwave LOS/NLOS radio link. A microwave terrestrial microwave LOS/NLOS radio link designer starts the design process by performing a link budget analysis. This entails a calculation involving the gains of antennas and path losses both in clear-air and rainfall conditions as well as noise and interference contributions. The path losses here include attenuation due to atmospheric effects including multipath, diffraction fading due to obstructions of the path profile, and miscellaneous losses due to couplings at the receiver and transmitter sites in addition to the free space path loss. The analysis must take into consideration the effective isotropic radiated power, *EIRP* from the transmitter, and all the losses just before the receiver. The fade margin calculated from the link budget calculation is used to determine the link availability under a variety of fading conditions. At the receiver, the designer needs to also consider receiver sensitivity. Below the receiver threshold noise level, no signal can be recovered. Each of the elements in the link budget calculation is discussed below:

4.1.1 Free Space Loss

A free space path loss provides a means to predict the received signal power when there is no object obstructing in the LOS path between the transmitter and the receiver sites. In line of sight radio systems, losses are mainly due to free space path loss. As the electromagnetic wave propagates between two geometrically separate points, its energy strength reduces with distance even if the path is a clear of obstacles. In that case of the LOS environment, the received power can fall off with the square of the distance between the transmitter and the receiver sites. For this idealistic scenario, the received power is simply given by Friis transmission equation as [25]:

$$l_{FSL} = \frac{P_{receiver}}{P_{transmitted}} = G_{TX}G_{RX}(\frac{\lambda}{4\pi d})^2 \tag{4.1}$$

where

G_{TX} is the gain of the transmitter antenna in dBi,

G_{RX} is the gain of the receiver antenna in dBi,

λ is wavelength of the transmission in meters,

d is the distance between the transmitter and receiver sites in km.

For simplicity, the basic free space loss assumes unity gain for both transmitting and receiving antennas, and is written as [31]:

$$L_{FSL} = 92.45 + 20log(d) + 20log(f) \tag{4.2}$$

where frequency and distance are in GHz and km, respectively.

P_aG_a multiplication is called *EIRP*, equivalent isotropically radiated power. It gives the power radiation at a fixed angle with respect to the isotropic antenna. But since isotropic antenna is not realistic, sometimes the power is given in terms of *ERP*, equivalent radiated power. *ERP* contains of all gain and loss factors for both transmitter and receiver sites, and usually expressed in dBm. If P_a is multiplied with numerical gain with respect to the isotropic antenna, EIRP value is found. So, gain value of an antenna is given in terms of dBi which is dB gain of antenna with respect to the isotropic antenna, or dBd which is dB gain of antenna with respect to the half wave dipole. We can write EIRP= ERP + 2.15 (dBi) since dipole has 2.15 dBi gain.

4.1.2 Received Power

The available signal power at the receiver site according to direct signal without the effect of the ground reflection is expressed by the following relation in dBm:

$$P_r = TX_{power} + G_{TX} + G_{RX} - CableLosses - (FSL + A_{gas} + A_{rain} + A_{diff}) \quad (4.3)$$

where

TX_{power} is the transmitted power in dBm,

G_{TX} is the gain of the transmitting antenna in dBi,

G_{RX} is the gain of the receiving antenna in dBi,

FSL is the free space loss in dB,

A_{gas} is the attenuation due to gases calculated by using formula of Eq. (3.1),

A_{rain} is the attenuation due to rain exceeded for p% of the time on a path of length in dB calculated by using formula of Eq. (3.8),

A_{diff} is the diffraction loss in dB.

Multipath fading is an important constraint on the prediction of path loss for terrestrial line-of-sight microwave links. When the reflected ray reaches the receiver at the same time as the directed ray, then, they can either add destructively or constructively resulting in signal attenuation or signal enhancement, respectively. Multipath fading normally gives rise to short-term outages. So, the total received power with the effect of the ground reflection is given by:

$$P_{total} = 10\,log(10^{\frac{P_r}{10}} \times (1 - 10^{\frac{-min(L_s)}{20}}))\ (dBm) \quad (4.4)$$

where L_s are the reflection losses of all reflection points along the terrestrial path profile in dB.

4.1.3 Noise Power

One of the limitations of the reception quality is noise. The noise power is given by [11]:

$$P_N = kT_eB \quad (4.5)$$

where k is the Boltzmann's constant= 1.38×10^{-23}, T_e is the ambient noise temperature in Kelvin of the environment in which the device operates; it is usually taken to be 290^o, and B is the equivalent bandwith of the link in Hertz.

4.1.4 Coherence Bandwidth

Multipath fading parameters are derived from the total received power. Most common descriptive parameters are *mean excess delay*, *rms delay spread* and *excess delay spread*. These parameters are called as time dispersion parameters due to excess time delays of each different path along the path profile. Mean, $\bar{\tau}$ and variance, $\bar{\tau}^2$ excess delay and rms delay spread, σ_τ are given by [25]:

$$\bar{\tau} = \frac{\sum_i P(\tau_i)\tau_i}{\sum_i P(\tau_i)} \tag{4.6}$$

$$\bar{\tau}^2 = \frac{\sum_i P(\tau_i)\tau_i^2}{\sum_i P(\tau_i)} \tag{4.7}$$

$$\sigma_\tau = \sqrt{\bar{\tau}^2 - (\bar{\tau})^2} \tag{4.8}$$

Within the coherence bandwidth, B_c all frequency components of the transmitted signal are affected approximately the same, i.e., they undergo the same attenuation and experience a linear phase shift. For frequency correlation function above 0.5, coherence bandwidth is given by [25]:

$$B_c \cong \frac{1}{5\sigma_\tau} \tag{4.9}$$

If the propagation path does not have any reflection points along the terrain path profile, the coherence bandwidth can become infinity.

4.1.5 Fade Margin

The fade margin is derived from the link budget calculation, and this parameter is then used to find the link availability in the terrestrial microwave LOS/NLOS radio link. Fade margin, also called link margin is a measure of how much margin is available in the communication link between the functional point and the point where the link can no longer be available. The fade margin calculation is given by:

$$A = P_{total} - P_N - SNR \tag{4.10}$$

where

P_{total} is the received power in dBm calculated by using formula of Eq. (4.4),
P_N is the noise power in dBm calculated by using formula of Eq. (4.5),
SNR is target signal-to-noise ratio in dB,
A is the fade margin in dB.

When the fade margin is negative, the signal is received under the specified bit error rate, or an average worst month outage could occur. The link margin is related to the link outage probability.

4.1.6 Link Availability

The link availability is the percent of time averaged over a month or a year. The link availability is calculated by using formula of Eq. (2.5) or (2.8) as a function of the fade margin. Many fixed microwave radio links are designed to be available essentially at all times. Usually, link availability of 99.99% for the worst month is the design goal for fixed links. This implies an outage not exceeding 52.56 minutes in a year. This equivalent link availability level is also referred to by the shorthand term four nines or 99.99%. The following table summarizes the outage time per year allowed for given availability percentages.

Availability (1-p)	Unavailability (p)	Outage per year
99%	1%	3.65 days
99.9%	0.1%	8.76 hours
99.99%	0.01%	52.56 minutes
99.999%	0.001%	315.36 seconds

Table 4.1: The outage time per year allowed for given link availability.

4.2 Path Profile and Simulation Studies

A path profile is defined as a geographical representation in two dimensions of the path followed by the radio beam between the two ends of a radio link. Path profile helps in determining the elevation height above sea level, and location of the transmitting and receiving antennas at each of the fixed microwave radio links. A path profile between transmitter and receiver sites generated using a Digital Terrain Elevation Data (*DTED 1*) [32] that has a post spacing with 3-arc seconds or an approximately 100 meters. Once the path profile is drawn, the preceding information can be used to adjust the terrain path profile for Earth bulge and k-factor variations. Table A.1 (Appendix A) provides an indication of the k factor values for different atmospheric refractive conditions. A typical example of a path profile with k-factor is shown in Fig. A.2.

Fig. 4.2 and 4.3 indicate base station sites for fixed terrestrial microwave LOS/NLOS radio links studied in both Istanbul and Ankara, Turkey. We applied simulations on terrestrial microwave LOS/NLOS radio links located in Istanbul and Ankara, Turkey. Two of these microwave radio links are LOS path case: Kazan-Elmadag and Fenertepe-Sazlıtepe, respectively. The other microwave radio links are NLOS or transhorizon path case such as Polatlı-Hüseyingazi and Dikmen-Polatlı, respectively. The main input parameters of these links are summarized in Table 4.2, 4.5, 4.8 and 4.12. The terrain path profiles of the terrestrial microwave LOS/NLOS radio links are presented in Fig. 2.6, 4.4, 4.5 and 4.6.

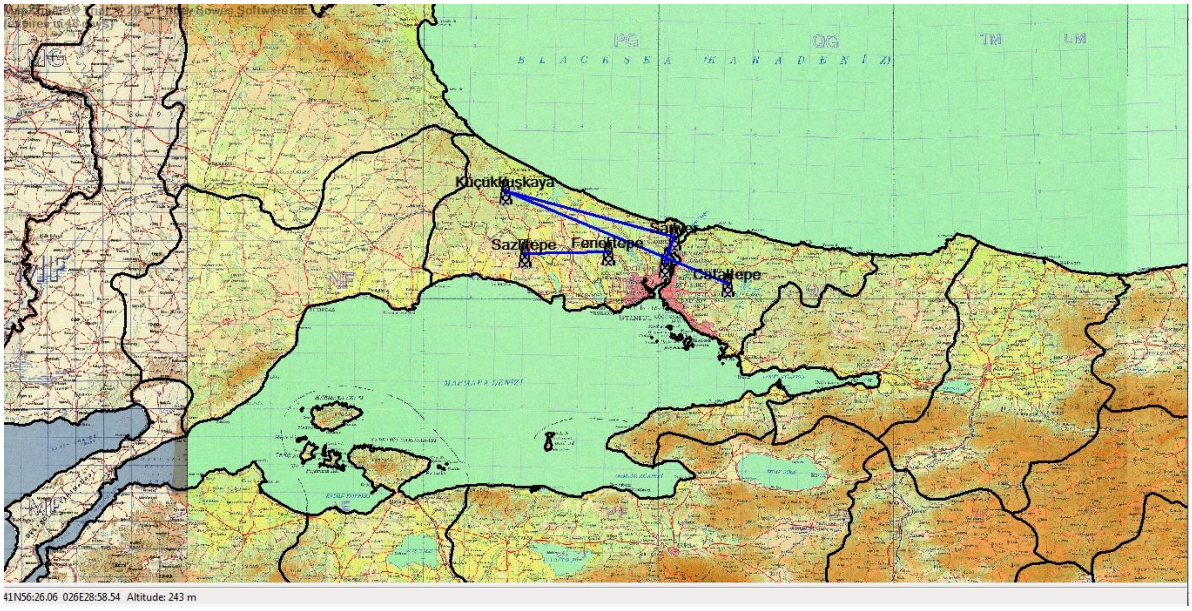

Figure 4.2: Location of sites used for microwave link simulations in Istanbul.

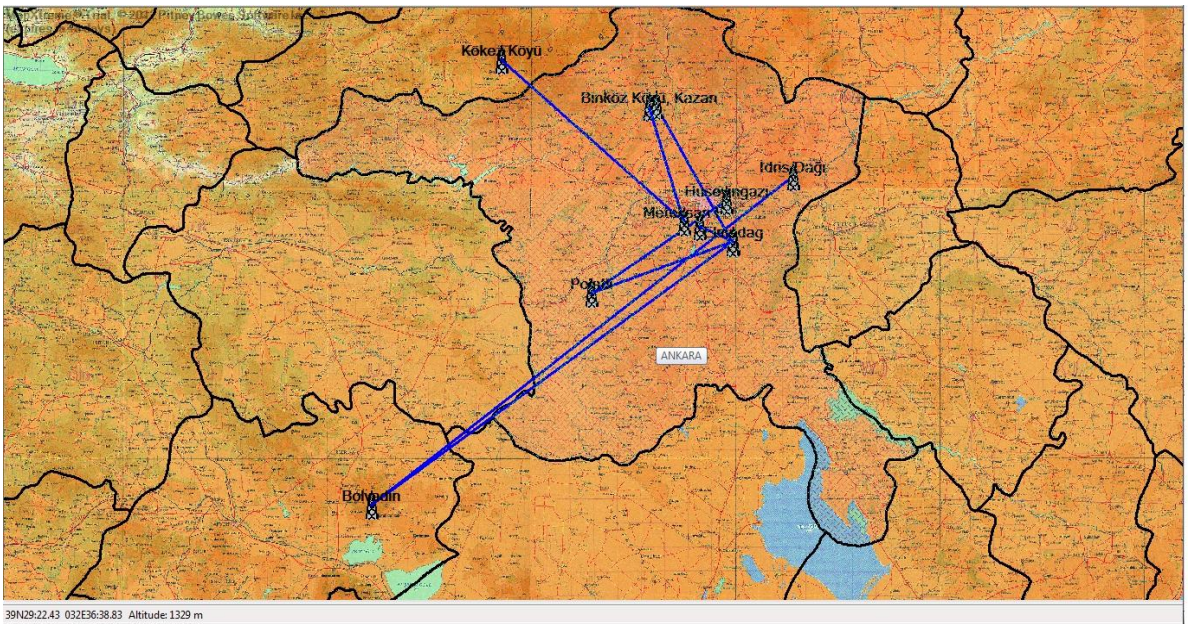

Figure 4.3: Location of sites used for microwave link simulations in Ankara.

4.2.1 Kazan-Elmadag Microwave R/L Case Study

A comparison of the results of the link simulation analysis as a function of the different polarizations are given in Table 4.3 and 4.4. It is a strongly LOS radio link because both transmitter and receiver sites are situated on top of hill, and the 0.6 First Fresnel zone is quite clear. So, the diffraction loss for this terrestrial microwave LOS radio link is 0 dB. For rain and atmospheric gases, Rec. ITU-R P.530 model seems less severe for operating frequencies below 5 GHz. There are relevant surface reflection points along the terrain path profile, and the diffuse reflection coefficient for vertical polarization is less than the coefficient for horizontal polarization in the same frequency. So, it is advantageous to chooce vertical polarization over horizontal polarization with regards to the total received power, and it is more likely to satisfy 99.99% worst month link availability criteria compared with horizontal polarization case.

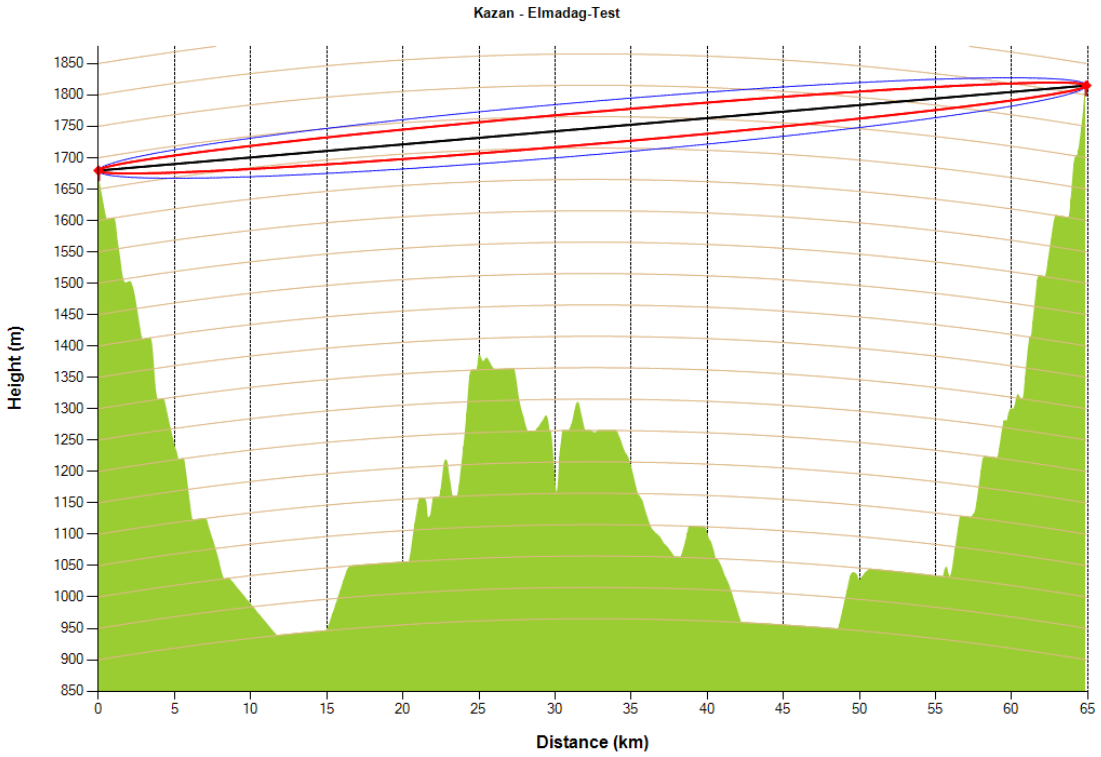

Figure 4.4: Terrain path profile of Kazan-Elmadag microwave LOS radio link (Frequency: 2 GHz, TX&RX Antenna Heights: 15 m a.g.l).

Parameter	**Kazan-Elmadag Microwave R/L**
Transmitter station, Kazan	40^o N $18^{'}$ $37.60^{"}$ 32^o E $36^{'}$ $43.00^{"}$
Receiver station, Elmadag	39^o N $48^{'}$ $3.30^{"}$ 32^o E $59^{'}$ $2.00^{"}$
Altitude of transmitter station (a.s.l)	1680 m
Altitude of receiver station (a.s.l)	1840 m
TX&RX antenna heights (a.g.l)	15 m
Radio frequency	1.350, 2 and 2.690 GHz
Transmitted power	25 dBm
TX&RX antenna gains	22 dBi
HPBW	10^o for 1.350 GHz 8^o for 2 GHz 6^o for 2.690 GHz
Cablo loss (for each site)	1 dB
Target SNR	6.95 dB
Bandwith	40 MHz
Diffraction method	Delta-Bullington
Time percentage for rain attenuation	0.01%
Polarization type	Vertical and Horizontal
Ground type	Medium Dry Ground
Season type	Winter

Table 4.2: Terrestrial link parameters for Kazan-Elmadag microwave LOS radio link.

Parameter	**Kazan-Elmadag Microwave R/L**
Azimuth	150.69^o
Path inclination	2.475 mrad
Minimum LOS clearance	61m, 1.00 km from Kazan site
Free space loss	131.35 dB for 1.350 GHz 134.77 dB for 2.0 GHz 137.34 dB for 2.690 GHz
Attenuation due to atmospheric gases	0.37 dB for 1.350 GHz 0.40 dB for 2.0 GHz 0.41 dB for 2.690 GHz
Attenuation due to rain	0.11 dB for 1.350 GHz 0.13 dB for 2.0 GHz 0.18 dB for 2.690 GHz
Diffraction loss	0 dB
Attenuation due to reflection loss	3.726 dB for 1.350 GHz 3.667 dB for 2.0 GHz 3.545 dB for 2.690 GHz
Total received power	-68.55 dBm for 1.350 GHz -71.97 dBm for 2.0 GHz -74.48 dBm for 2.690 GHz
Noise power	-97.95 dBm
Fade margin	22.45 dB for 1.350 GHz 19.04 dB for 2.0 GHz 16.52 dB for 2.690 GHz
Link availability	99.9976% for 1.350 GHz 99.9931% for 2.0 GHz 99.9841% for 2.690 GHz

Table 4.3: Results of link simulation as a function of vertical polarization on Kazan-Elmadag terrestrial microwave LOS radio link.

Parameter	**Kazan-Elmadag Microwave R/L**
Azimuth	150.69^o
Path inclination	2.475 mrad
Minimum LOS clearance	61m, 1.00 km from Kazan site
Free space loss	131.35 dB for 1.350 GHz 134.77 dB for 2.0 GHz 137.34 dB for 2.690 GHz
Attenuation due to atmospheric gases	0.37 dB for 1.350 GHz 0.40 dB for 2.0 GHz 0.42 dB for 2.690 GHz
Attenuation due to rain	0.09 dB for 1.350 GHz 0.13 dB for 2.0 GHz 0.19 dB for 2.690 GHz
Diffraction loss	0 dB
Attenuation due to reflection loss	5.051 dB for 1.350 GHz 4.956 dB for 2 GHz 4.762 dB for 2.690 GHz
Total received power	-69.86 dBm for 1.350 GHz -73.25 dBm for 2.0 GHz -75.71 dBm for 2.690 GHz
Noise power	-97.95 dBm
Fade margin	21.14 dB for 1.350 GHz 17.75 dB for 2.0 GHz 15.29 dB for 2.690 GHz
Link availability	99.9968% for 1.350 GHz 99.9906% for 2.0 GHz 99.9783% for 2.690 GHz

Table 4.4: Results of link simulation as a function of horizontal polarization on Kazan-Elmadag terrestrial microwave LOS radio link.

4.2.2 Fenertepe-Sazlıtepe Microwave R/L Case Study

Table 4.6 and 4.7 have provided the results of the link simulation analysis in different polarizations on Fenertepe-Sazlıtepe microwave LOS radio link. It is also a strongly LOS radio link because the 60% of the first Fresnel zone's radius is kept clear, and the diffraction propagation mechanism is negligible in that case. The analysis of overall performance in terms of the worst month link availability over the two terrestrial microwave LOS radio links (Kazan-Elmadag and Fenertepe-Sazlıtepe radio links) shows clearly that these links comply with 99.99% worst month link availability criteria.

Parameter	**Fenertepe-Sazlıtepe Microwave R/L**
Transmitter station, Fenertepe	41^o N $09^{'}$ $2.40^{"}$ 28^o E $47^{'}$ $9.60^{"}$
Receiver station, Sazlıtepe	41^o N $08^{'}$ $43.40^{"}$ 28^o E $25^{'}$ $43.80^{"}$
Altitude of transmitter station (a.s.l)	224 m
Altitude of receiver station (a.s.l)	340 m
Antenna height (a.g.l), Fenertepe	4 m
Antenna height (a.g.l), Sazlıtepe	18 m
Radio frequency	1.350, 2 and 2.690 GHz
Transmitted power	22 dBm
TX&RX antenna gains	24 dBi
HPBW	10^o for 1.350 GHz 8^o for 2 GHz 6^o for 2.690 GHz
Cablo loss (for each site)	1 dB
Target SNR	6.95 dB
Bandwith	20 MHz
Diffraction method	Delta-Bullington
Time percentage for rain attenuation	0.01%
Polarization type	Vertical and Horizontal
Ground type	Medium Dry Ground
Season type	Winter

Table 4.5: Terrestrial link parameters for Fenertepe-Sazlıtepe microwave LOS radio link.

Parameter	**Fenertepe-Sazlıtepe Microwave R/L**
Azimuth	268.95^o
Path inclination	4.264 mrad
Minimum LOS clearance	5m, 0.40 km from Fenertepe site
Free space loss	124.57 dB for 1.350 GHz 127.98 dB for 2.0 GHz 130.56 dB for 2.690 GHz
Attenuation due to atmospheric gases	0.21 dB for 1.350 GHz 0.23 dB for 2.0 GHz 0.24 dB for 2.690 GHz
Attenuation due to rain	0.09 dB for 1.350 GHz 0.23 dB for 2.0 GHz 0.30 dB for 2.690 GHz
Diffraction loss	0 dB
Attenuation due to reflection loss	5.803 dB for 1.350 GHz 5.7605 dB for 2 GHz 5.6691 dB for 2.690 GHz
Total received power	-63.08 dBm for 1.350 GHz -66.20 dBm for 2.0 GHz -68.77 dBm for 2.690 GHz
Noise power	-100.96 dBm
Fade margin	30.94 dB for 1.350 GHz 27.81 dB for 2.0 GHz 25.24 dB for 2.690 GHz
Link availability	99.9998% for 1.350 GHz 99.9971% for 2.0 GHz 99.9934% for 2.690 GHz

Table 4.6: Results of link simulation as a function of vertical polarization on Fenertepe-Sazlıtepe terrestrial microwave LOS radio link.

Parameter	**Fenertepe-Sazlıtepe Microwave R/L**
Azimuth	268.95^o
Path inclination	4.264 mrad
Minimum LOS clearance	5m, 0.40 km from Fenertepe site
Free space loss	124.57 dB for 1.350 GHz 127.98 dB for 2.0 GHz 130.56 dB for 2.690 GHz
Attenuation due to atmospheric gases	0.21 dB for 1.350 GHz 0.23 dB for 2.0 GHz 0.24 dB for 2.690 GHz
Attenuation due to rain	0.10 dB for 1.350 GHz 0.23 dB for 2.0 GHz 0.31 dB for 2.690 GHz
Diffraction loss	0 dB
Attenuation due to reflection loss	7.3454 dB for 1.350 GHz 7.2778 dB for 2 GHz 7.1359 dB for 2.690 GHz
Total received power	-64.64 dBm for 1.350 GHz -67.72 dBm for 2.0 GHz -70.25 dBm for 2.690 GHz
Noise power	-100.96 dBm
Fade margin	29.38 dB for 1.350 GHz 26.29 dB for 2.0 GHz 23.77 dB for 2.690 GHz
Link availability	99.9985% for 1.350 GHz 99.9959% for 2.0 GHz 99.9910% for 2.690 GHz

Table 4.7: Results of link simulation as a function of horizontal polarization on Fenertepe-Sazlıtepe terrestrial microwave LOS radio link.

4.2.3 Polatlı-Hüseyingazi Microwave R/L Case Study

The path loss predictions are carried out at 1.350, 2.0 and 2.690 GHz frequencies with a height of 35 m above ground level. It is a NLOS radio link because there is one obstacle over the LOS line in the first Fresnel ellipsoid. From the Table 4.8, choice of different diffraction propagation methods plays predominant role in the calculation of the predicted path loss values on Polatlı-HüseyinGazi microwave NLOS radio link. As shown in Table 4.10 and 4.11, Delta-Bullington method overestimates the diffraction loss value due to the correction term, and so it is less likely to satisfy 99.99% worst month link availability criteria in NATO Band 3+ frequency band. In addition, there are no relevant surface reflection points along the path profile. So, choice of different polarization types can not affect the value of the total received power over the terrestrial microwave NLOS radio link.

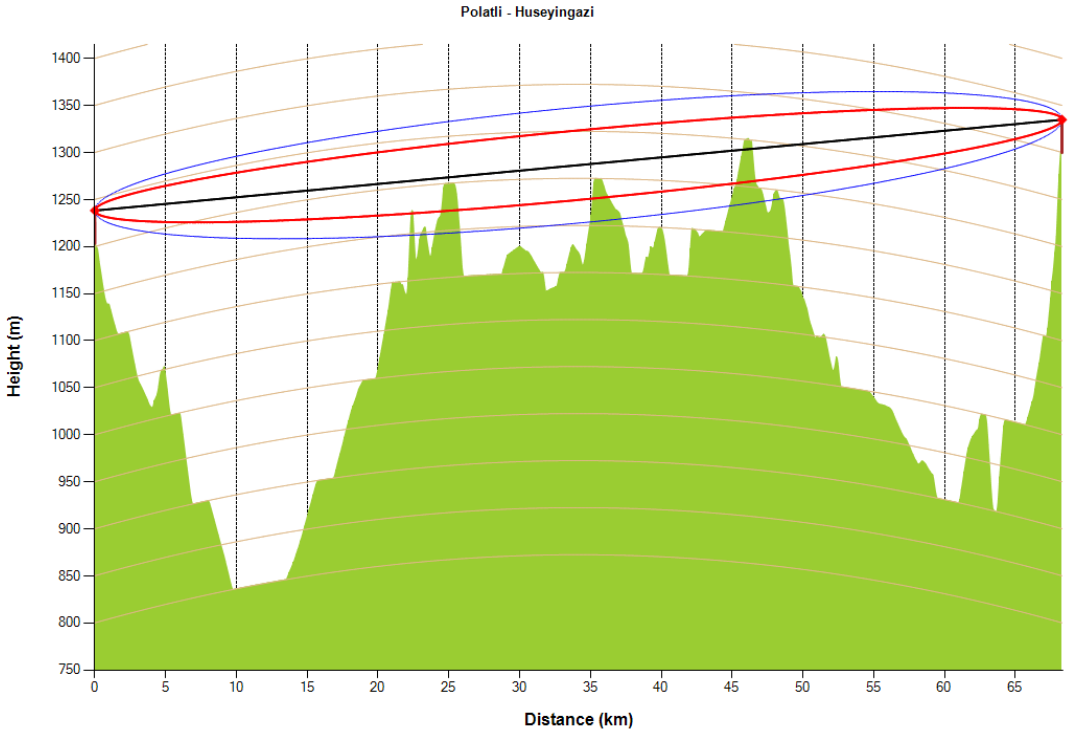

Figure 4.5: Terrain path profile of Polatlı-Hüseyingazi microwave NLOS radio link (Frequency: 1.35 GHz, TX&RX Antenna Heights: 35 m a.g.l).

Parameter	**Polatlı-Hüseyingazi Microwave R/L**
Transmitter station, Polatlı	39^o N $36^{'}$ $38.00^{"}$ 32^o E $17^{'}$ $35.00^{"}$
Receiver station, Hüseyingazi	39^o N $57^{'}$ $17.00^{"}$ 32^o E $57^{'}$ $18.00^{"}$
Altitude of transmitter station (a.s.l)	1238 m
Altitude of receiver station (a.s.l)	1325 m
TX&RX antenna heights (a.g.l)	35 m
Radio frequency	1.350, 2 and 2.690 GHz
Transmitted power	20 dBm
TX&RX antenna gains	27.15 dBi
HPBW	10^o for 1.350 GHz 8^o for 2 GHz 6^o for 2.690 GHz
Cablo loss (for each site)	3.6 dB
Target SNR	4.95 dB
Bandwith	20 MHz
Diffraction method	Delta-Bullington, Epstein-Peterson and Deygout
Time percentage for rain attenuation	0.01%
Polarization type	Vertical and Horizontal
Ground type	Very Dry Ground
Season type	Winter

Table 4.8: Terrestrial link parameters for Polatlı-Hüseyingazi microwave NLOS radio link.

Parameter	**Polatlı-Hüseyingazi Microwave R/L**
Azimuth	150.69^o
Path inclination	2.475 mrad
Minimum LOS clearance	-11m, 46.06 km from Site1
Free space loss	131.79 dB for 1.350 GHz 135.21 dB for 2.0 GHz 137.78 dB for 2.690 GHz
Attenuation due to atmospheric gases	0.39 dB for 1.350 GHz 0.43 dB for 2.0 GHz 0.44 dB for 2.690 GHz
Attenuation due to rain	0.13 dB for 1.350 GHz 0.15 dB for 2.0 GHz 0.20 dB for 2.690 GHz
Diffraction loss	13.89 dB for 1.350 GHz 14.73 dB for 2 GHz 15.49 dB for 2.690 GHz
Attenuation due to reflection loss	0 dB
Total received power	-79.11 dBm for 1.350 GHz -83.42 dBm for 2.0 GHz -86.82 dBm for 2.690 GHz
Noise power	-100.96 dBm
Fade margin	16.91 dB for 1.350 GHz 12.60 dB for 2.0 GHz 9.19 dB for 2.690 GHz
Link availability	99.9724% for 1.350 GHz 99.8951% for 2.0 GHz 99.6712% for 2.690 GHz

Table 4.9: Results of link simulation for both horizontal and vertical polarizations on Polatlı-Hüseyingazi terrestrial microwave NLOS radio link (by using only Delta-Bullington diffraction method).

Frequency	**Delta-Bullington, dB**	**Deygout and Epstein-Peterson, dB**
1.350 GHz	13.89	8.43
2.0 GHz	14.73	8.95
2.690 GHz	15.49	15.49

Table 4.10: Results of predicted diffraction loss for three diffraction prediction methods on Polatlı-Hüseyingazi terrestrial microwave NLOS radio link.

Frequency	**Delta-Bullington, dBm**	**Deygout and Epstein-Peterson, dBm**
1.350 GHz	-79.11	-73.65
2.0 GHz	-83.42	-77.63
2.690 GHz	-86.82	-86.82

Table 4.11: Results of predicted received power for three diffraction prediction methods on Polatlı-Hüseyingazi terrestrial microwave NLOS radio link.

4.2.4 Dikmen-Polatlı Microwave R/L Case Study

The results of link simulation analysis as a function of different diffraction methods on Dikmen-Polatlı microwave NLOS radio link is given in Table 4.13. It is also a strongly NLOS radio link because the 60% of the first Fresnel zone's radius is not kept clear, and there are two obstacles over the LOS line along the terrain path profile. If the calculated diffraction loss over the terrain is greater than about 15 dB mentioned in Rec. ITU-R P.530, the diffraction loss formula for all diffraction methods can be the same, and Dikmen-Polatlı microwave NLOS radio link can satisfy 99.99% worst month link availability criteria only in 1.350 GHz frequency. Moreover, there are no relevant surface reflection points along the path profile. So, attenuation due to reflection loss is 0 dB.

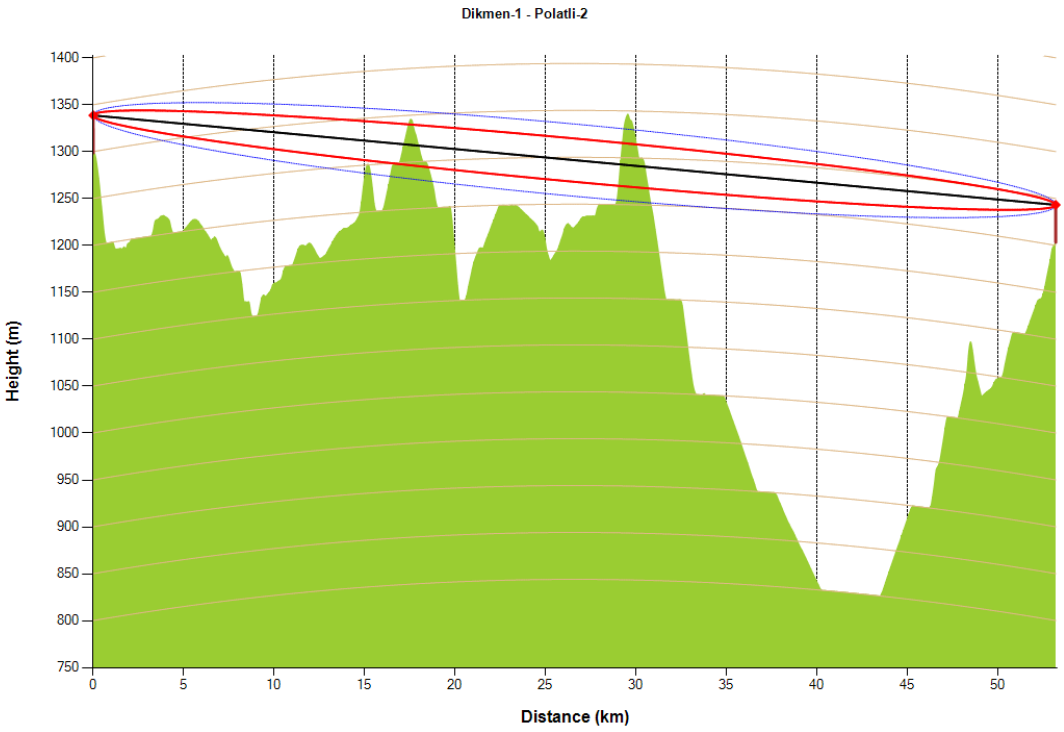

Figure 4.6: Terrain path profile of Dikmen-Polatlı microwave NLOS radio link (Frequency: 2.690 GHz, TX&RX Antenna Heights: 40 m a.g.l).

Parameter	**Dikmen-Polatlı Microwave R/L**
Transmitter station, Dikmen	39^o N $51^{'}$ $32.00^{"}$ 32^o E $49^{'}$ $29.00^{"}$
Receiver station, Polatlı	39^o N $36^{'}$ $38.00^{"}$ 32^o E $17^{'}$ $35.00^{"}$
Altitude of transmitter station (a.s.l)	1339 m
Altitude of receiver station (a.s.l)	1243 m
TX&RX antenna heights (a.g.l)	40 m
Radio frequency	1.350, 2 and 2.690 GHz
Transmitted power	30 dBm
TX&RX antenna gains	27.15 dBi
HPBW	10^o for 1.350 GHz 8^o for 2 GHz 6^o for 2.690 GHz
Cablo loss (for each site)	1 dB
Target SNR	4.95 dB
Bandwith	20 MHz
Diffraction method	Delta-Bullington, Epstein-Peterson and Deygout
Time percentage for rain attenuation	0.01%
Polarization type	Vertical and Horizontal
Ground type	Very Dry Ground
Season type	Winter

Table 4.12: Terrestrial link parameters for Dikmen-Polatlı microwave NLOS radio link.

Parameter	**Dikmen-Polatlı Microwave R/L**
Azimuth	238.90^o
Path inclination	-1.793 mrad
Minimum LOS clearance	-54m, 29.55 km from Dikmen site
Free space loss	129.62 dB for 1.350 GHz 133.04 dB for 2.0 GHz 135.61 dB for 2.690 GHz
Attenuation due to atmospheric gases	0.30 dB for 1.350 GHz 0.33 dB for 2.0 GHz 0.34 dB for 2.690 GHz
Attenuation due to rain	0.10 dB for 1.350 GHz 0.23 dB for 2.0 GHz 0.25 dB for 2.690 GHz
Diffraction loss (for all diffraction methods)	30.09 dB for 1.350 GHz 34.46 dB for 2 GHz 38.36 dB for 2.690 GHz
Attenuation due to reflection loss	0 dB
Total received power (for all diffraction methods)	-77.82 dBm for 1.350 GHz -85.76 dBm for 2.0 GHz -92.27 dBm for 2.690 GHz
Noise power	-100.96 dBm
Fade margin (for all diffraction methods)	18.19 dB for 1.350 GHz 10.26 dB for 2.0 GHz 3.75 dB for 2.690 GHz
Link availability (for all diffraction methods)	99.9920% for 1.350 GHz 99.9050% for 2.0 GHz 97.6809% for 2.690 GHz

Table 4.13: Results of link simulation for both horizontal and vertical polarizations on Dikmen-Polatlı terrestrial microwave NLOS radio link.

Chapter 5

VALIDATION AND COMPARISON OF RESULTS

In this section, the implementation of link analysis for the design of fixed terrestrial point-to-point systems is justified by comparison with the commercial ATDI ICS telecom software [8] and the measurement data existing in the literature [9,10] over sample fixed terrestrial microwave LOS/NLOS radio links. The short-term diffraction measurements during August and September 2012 were performed in the area of Czech Republic with the use of truck-mounted access platform reaching up to 46 meters above ground level mentioned in [9, 10] papers. This chapter is divided into two sections. The first section compares the performance of the fixed terrestrial microwave LOS radio link in terms of the total received power with the commercial ATDI ICS telecom software. In the second section, we have done a comparative case studies between Delta-Bullington diffraction method and the obtained measurement data [9,10] over the sample fixed terrestrial microwave LOS/NLOS radio links.

5.1 Comparison with the ATDI ICS Telecom Software

We have compared the overall performance in terms of the total received power over some microwave LOS radio links with the commercial ATDI ICS telecom software [8]. To verify the implementation of link analysis in the terrestrial microwave radio link, we applied simulations on terrestrial microwave LOS radio links located in Ankara, Turkey. To reduce the number of figures, we present only one sample case study which illustrated results of both the implementation of link analysis and other model via the commercial ATDI ICS telecom software. Detail terrain profile containing information about actual terrain profile (green), the first Fresnel zone (red) and line-of-sight line (purple) is obtained by using the ATDI ICS telecom software, as can be seen in Fig. 5.1.

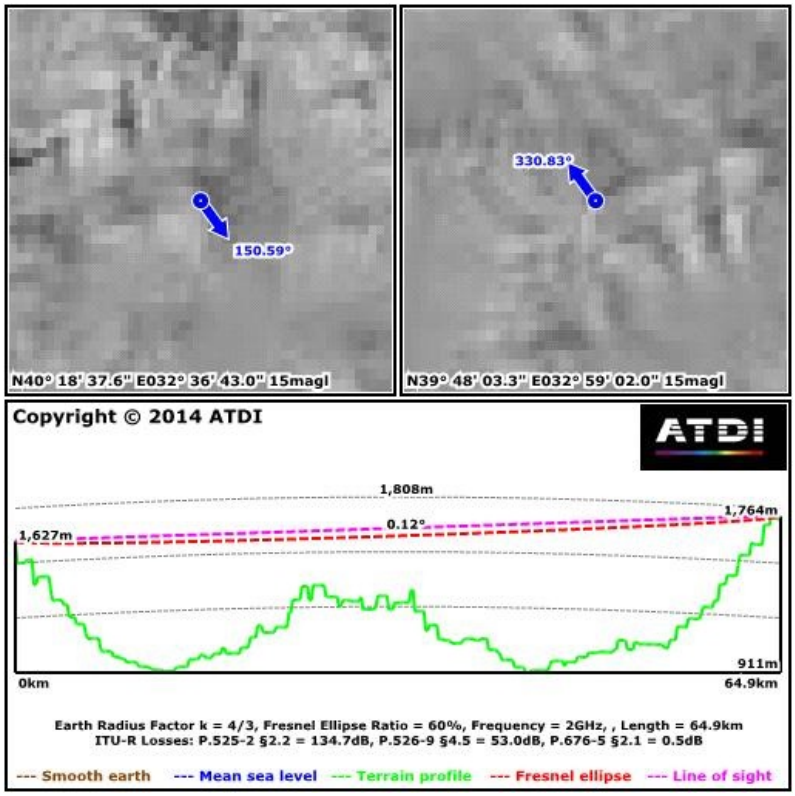

Figure 5.1: Kazan-Elmadag microwave LOS radio link profile over terrain with the terrain elevations above sea level adjusted for 4/3 effective Earth radius curvature by the ATDI ICS telecom software.

A 64.9 kilometer path from Kazan (N 40^o $18^{'}$ $37.6^{"}$, E 32^o $36^{'}$ $43^{"}$) to Elmadag (N 39^o $48^{'}$ $3.3^{"}$, E 32^o $59^{'}$ $2^{"}$) was selected for the case study as shown in Fig. 5.1. Kazan antenna height is 1665 m a.s.l, and Elmadag antenna height is 1825 m a.s.l. The expected rain intensity for 0.01% of the time in this area is 27.66 mm/h. The link is between Kazan and Elmadag in Turkey with the following link parameters as shown in Table 5.1. The obtained results are also summarized in Table 5.2 and 5.3.

The validity of the implementation of link analysis is justified by comparison with the commercial ATDI ICS telecom software over sample microwave LOS/NLOS radio links located in Turkey. The analysis of overall performance in terms of the total received power over sample microwave LOS radio link shows that the method is compatible with the other model via ATDI ICS telecom software.

Parameter	**Kazan-Elmadag Microwave R/L**
Altitude of transmitter station (a.s.l)	1680 m
Altitude of receiver station (a.s.l)	1840 m
TX&RX antenna heights (a.g.l)	15 m
Radio frequency	2 GHz
Transmitted power	25 dBm
TX&RX antenna gains	22 dBi
HPBW	8^o
Cablo loss (for each site)	1 dB
Target SNR	6.95 dB
Bandwith	40 MHz
Diffraction method	Delta-Bullington
Time percentage for rain attenuation	0.01%
Polarization type	Vertical
Ground type	Medium Dry Ground
Season type	Winter

Table 5.1: Terrestrial link parameters for Kazan-Elmadag terrestrial microwave LOS radio link (validation case study).

Parameter	**Kazan-Elmadag Microwave R/L**
Azimuth	150.69^o
Path inclination	2.475 mrad
Minimum LOS clearance	61m, 1.00 km from Kazan site
Free space loss	134.77 dB
Attenuation due to atmospheric gases	0.40 dB
Attenuation due to rain	0.13 dB
Diffraction loss	0 dB
Attenuation due to reflection loss	3.667 dB
Total received power	-71.97 dBm

Table 5.2: Results of link simulation as a function of vertical polarization on Kazan-Elmadag terrestrial microwave LOS radio link (validation case study).

Parameter	**Kazan-Elmadag Microwave R/L**
Free space loss	134.7 dB
Attenuation due to atmospheric gases	0.50 dB
Attenuation due to rain (27.66 mm/h)	0.20 dB
Diffraction loss	0 dB
Attenuation due to reflection loss	3.0 dB
Total received power	-71.24 dBm

Table 5.3: Results of ATDI ICS telecom software on Kazan-Elmadag terrestrial microwave LOS radio link.

5.2 Experimental Validation of ITU-R Model for Terrestrial LOS/NLOS Microwave Links

The implementation of link analysis is compared with the measurement data existing in the literature [9, 10] over sample microwave LOS/NLOS radio links. The short-term terrain diffraction measurements during August and September 2012 were performed in the area of Czech Republic mentioned in [9, 10] papers. These trials were carried out for several combinations of transmitter and receiver heights at the frequencies of 2.0 GHz, 3.5 GHz and 5.0 GHz for the case of both the horizontal and vertical polarizations [9, 10]. Detailed information regarding two scenarios is provided in Table 5.4 [10]. The terrain path profiles of two scenarios are shown in Fig. 5.2 and 5.3. We have provided a comparison between Delta-Bullington diffraction method and the obtained measurement data [9, 10]. Fig. 5.4 presents diffraction loss scenario 1, both as measurement data [10], and as predicted by the Delta-Bullington diffraction method.

Scenario	**1**	**2**
Path length (km)	17.3	11.2
Transmitter station, latitude	50^o N $13^{'}$ $56.13^{"}$	50^o N $01^{'}$ $41.80^{"}$
Transmitter station, longitude	14^o E $01^{'}$ $59.22^{"}$	13^o N $34^{'}$ $58.63^{"}$
Receiver station, latitude	50^o N $10^{'}$ $53.36^{"}$	50^o N $03^{'}$ $23.43^{"}$
Receiver station, longitude	14^o E $15^{'}$ $43.54^{"}$	13^o N $44^{'}$ $00.41^{"}$
Altitude of transmitter station (a.s.l)	323 m	
Altitude of receiver station (a.s.l)	319 m	
TX antenna height (a.g.l)	9.8 m	
RX antenna height (a.g.l)	4.6-23.8 m	
Radio frequency	2, 3.5 and 5 GHz	

Table 5.4: Selected measurement scenarios.

Frequency	**2.0**	**3.5**	**5**
DRH18-E antenna gain (dBi)	9.8	11.7	11.4
Output power (dBm)	27.0	27.5	27.8
Cable loss at transmitter station (dB)	2.6	4.0	5.6
Cable loss at receiver station (dB)	2.8	3.1	3.4
Polarization	Vertical and Horizontal		

Table 5.5: System parameters at 2.0 GHz, 3.5 GHz and 5.0 GHz.

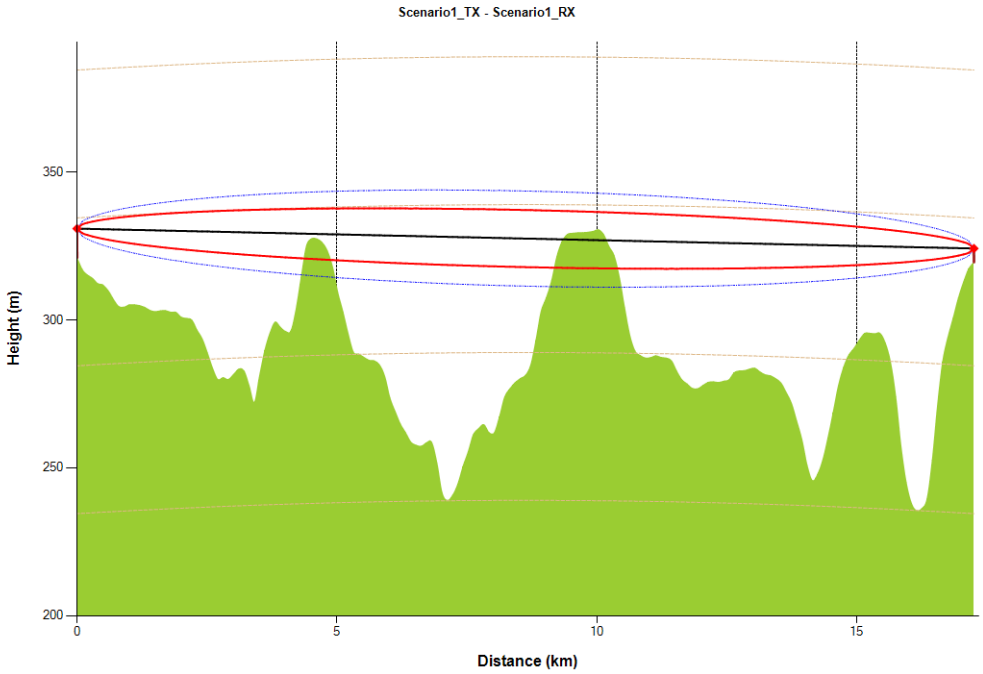

Figure 5.2: Terrain path profile of the scenario 1 (Frequency: 5 GHz, TX Antenna Height: 9.8 m a.g.l and RX Antenna Height: 4.6 m a.g.l).

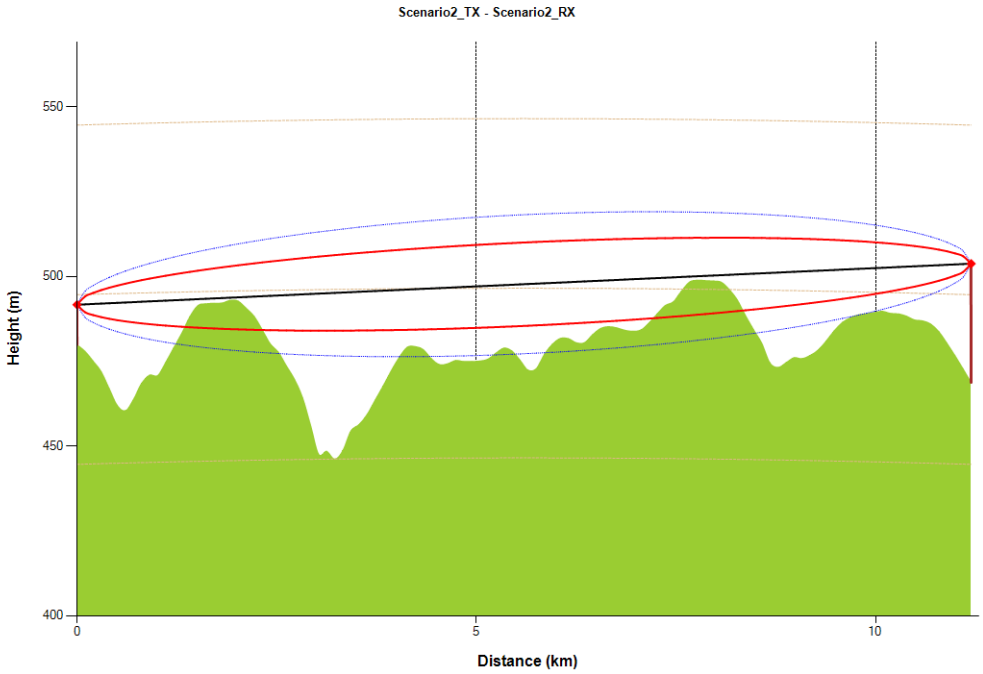

Figure 5.3: Terrain path profile of the scenario 2 (Frequency: 2 GHz, TX Antenna Height: 11.8 m a.g.l and RX Antenna Height: 35 m a.g.l).

Fig. 5.5 and 5.6 present the diffraction loss for the scenario 2 as obtained during the measurements [10] and by using the Delta-Bullington diffraction method for the transmitter antenna heights of 11.8 and 23.8 m a.g.l.

It can be seen from Fig. 5.4 that the difference between measurement and prediction is a small for the case of the receiver antenna height of 23.8 m a.g.l at 2 GHz frequency compared with the other cases. In addition, the Delta-Bullington method has overestimated the diffraction loss for the case of the receiver antenna height of 4.6 m a.g.l at 2 GHz frequency.

Based on the results presented Fig. 5.5 and 5.6, it can be stated that the diffraction loss is decreasing with increasing antenna height of the receiver station, as expected. Further, a very good match between measurements and predictions can be found for the highest antenna height of the receiver station, where even LOS propagation condition can be achieved for the case of transmitter antenna height of 23.8 m a.g.l. On the other hand, the differences between measurements and predictions are about 10 dB for the case of the lowest receiver antenna height.

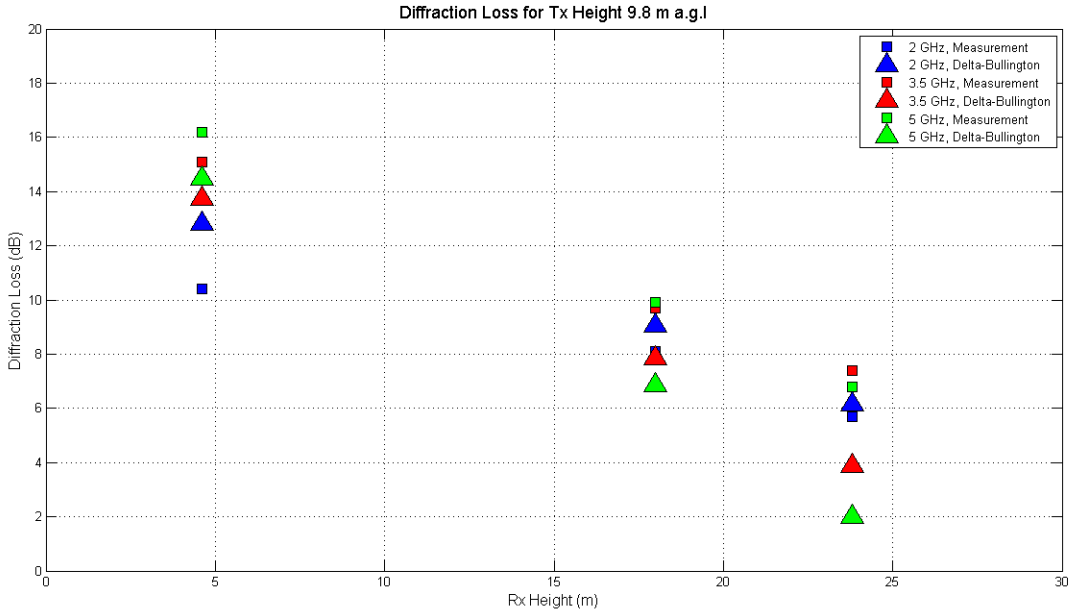

Figure 5.4: Path loss for the scenario 1 as abtained during the measurements and by using the Delta-Bullington diffraction method for the transmitter antenna height of 9.8 m a.g.l.

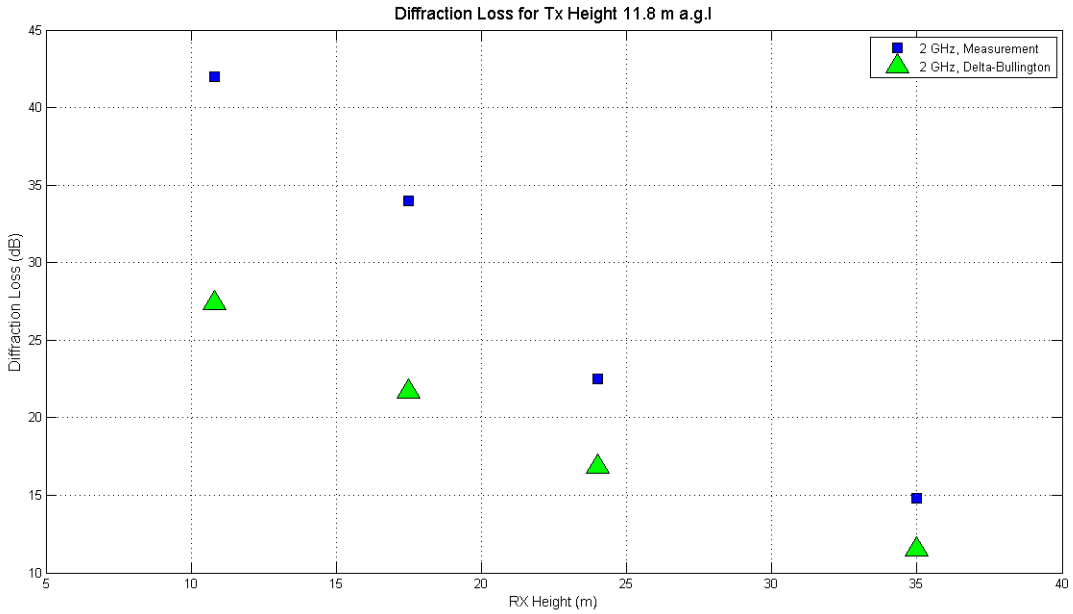

Figure 5.5: Path loss for the scenario 2 as abtained during the measurements and by using the Delta-Bullington diffraction method for the transmitter antenna height of 11.8 m a.g.l.

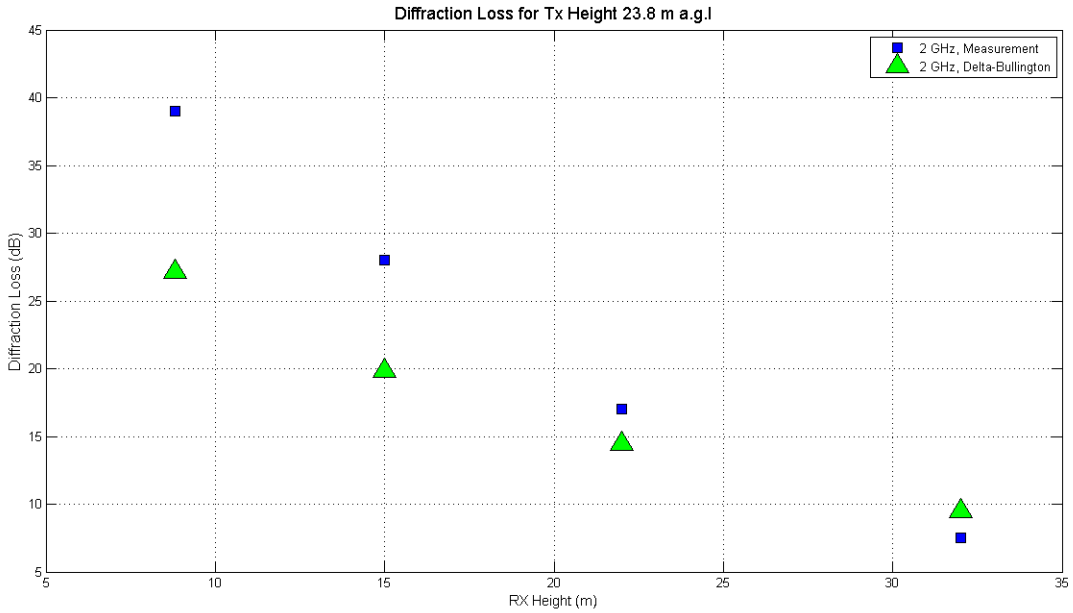

Figure 5.6: Path loss for the scenario 2 as abtained during the measurements and by using the Delta-Bullington diffraction method for the transmitter antenna height of 23.8 m a.g.l.

Chapter 6

CONCLUSION

In this thesis, propagation link analysis of fixed terrestrial point-to-point microwave LOS/NLOS radio systems for rural environment is studied. The performance analysis in terms of both total received power and link availability of fixed terrestrial microwave LOS/NLOS radio links have been simulated and evaluated. The worst month link availability is investigated for fixed terrestrial microwave LOS/NLOS radio links operating in NATO Band 3+ (1350-2690 MHz) and NATO Band 4 (4400-5000 MHz) frequency bands.

We have done a comparative analysis of the multipath propagation models presented by various authors, reviewed in Chapter 2. Based on our analysis and results, Rec. ITU-R P.530 accurately models the LOS/NLOS propagation in Turkey compared with the other models in the literature. The main reason can be attributed to the fact that Rec. ITU-R P.530 model has more climate and terrain parameters to design accurate fixed terrestrial microwave LOS/NLOS radio links. In addition, there is a flexibility K factor value due to dN_1 and S_a parameters in contrast to Q and C propagation factor values which are solely based on generic tables. The propagation conditions factor for Barnett-Vigants and Morita fading models could not consider any variations over Turkey, but propagation geoclimatic factor of Rec. ITU-R P.530 model varies based on refractivity gradient and terrain roughness parameters in Turkey. In addition, we compared

the overall performance of all multipath fading models in terms of total outage probability over the sample microwave radio link located in Turkey, and so Rec. ITU-R P.530 model is optimistic.

In Chapter 3, the multipath fading outage prediction method proposed by Rec. ITU-R P.530 model is studied. All significant clear-air and rainfall propagation mechanisms are introduced. These propagation mechnanisms are an important constraint on the prediction of path losses for fixed terrestrial microwave LOS/NLOS links at different frequencies. Attenuation due to atmospheric gases and rain are small for operating frequencies below 5 GHz, and thus often neglected in NATO Band 3+ and NATO Band 4 frequency bands. Diffraction phenomenon occurs when 60% of the first Fresnel zone is obstructed by an obstacle or several obstacles between the transmitter and receiver sites. The calculation of the diffraction loss is assuming as a knife-edge. If the propagation path consists of more than one single knife-edge obstruction, Rec. ITU-R P.526 model suggests Epstein-Peterson, Deygout and Delta-Bullington methods to calculate the total diffraction loss due to multiple knife-edges. However, the Epstein-Peterson and Deygout methods used only for two obstacles over the LOS line. Moreover, if none of the knife-edges are above the LOS, then Rec. ITU-R P.526 provides the calculation only on Delta-Bullington method for the diffraction losses. For this case, Delta-Bullington method is is not based on constructing an equivalent hypothetical single knife-edge at the intersection of transmitter and receiver sites. Alternatively, we have proposed a multiple knife-edge diffraction method for LOS line. If the propagation path consists of more than one obstruction over the LOS line, then our proposed gives the same result with the Delta-Bullington method. In addition, the calculation of reflection points on the terrain path profile is improved.

Chapter 4 provides the link budget calculation process in the defined terrestrial microwave LOS/NLOS radio link. The calculation of both the total received power with the effect of the ground reflection and the fade margin are developed to find the link availability in the terrestrial microwave LOS/NLOS radio link. To complete the microwave performance analysis, we applied simulations on terrestrial microwave LOS/NLOS radio links located in Istanbul and Ankara, Turkey.

According to the link study simulation results, if the terrain path profile is a LOS radio link, reflection mechanism plays a predominant role on the calculation of the received power in the terrestrial microwave LOS radio link, and diffraction fading plays prominent role on the calculation of the received power in another path profile case. In addition, the implementation of link analysis is compared by using the ATDI ICS telecom software and the measurement data existing in the literature over sample fixed terrestrial microwave LOS/NLOS radio links.

The future work will be focused on field measurements which will be used for better comparison of the results of the link analysis. Data for Turkey should be collected in the future, to further test and verify the prediction model developed in this work. Moreover, correlation study and analysis of interference mechanism should be done with the verification of the prediction model. Interference prediction method proposed by Rec. ITU-R P.452 model [33] will be studied.

Appendix A

Effective Earth Radius

The radio refractive index is the ratio of velocity of propagation of a radio wave in free space to the velocity in a specified medium. At standard atmospheric environments, the value of the radio refractive index, n has a value of about 1.000312. Therefore, a more convenient quantity, the atmospheric refractivity N (N-units) is usually used, and it is given by [21]:

$$N = (n - 1) \times 10^6 \tag{A.1}$$

Substituting the value for the ground refractive index (n = 1.000312) into Eqs. (A.1) yields a N value of 312 N-units. From ITU-R P. 453 [18], N can be modelled as:

$$N = \frac{77.6}{T}(P + 4810\frac{e}{T}) \tag{A.2}$$

where

P is the total atmospheric pressure in hPa,

e is the water vapour pressure in hPa,

T is the air temperature in degrees.

The value of N varies with altitude since relative humidity, temperature, and pressure all vary with height. So, pressure and humidity normally decrease exponentially with height above ground. Humidity and temperature do, however, change under certain conditions resulting in variations of radio refractivity.

In general, the atmosphere displays an exponential decrease of N with height. For the average atmosphere, refractivity can be written as [18]:

$$N(h) = N_o e^{-\frac{h}{h_o}} \tag{A.3}$$

where $N_o = 315$ N-units for standart atmosphere and for altitudes below 1 km, $h_o \cong 7$ km.

The refractivity gradient is defined as:

$$dN_1 = \frac{dN}{dh} \tag{A.4}$$

From Eq. (A.1), n=$(1+N \times 10^{-6})$ giving

$$\frac{\mathrm{d}n}{\mathrm{d}h} = \frac{\mathrm{d}N}{\mathrm{d}h} \times 10^{-6} \;\; N - units/km \tag{A.5}$$

and from Eq. (A.3),

$$\frac{\mathrm{d}N}{\mathrm{d}h} = -\frac{N_o}{h_o} exp(-1/7) \tag{A.6}$$

For heights less than 1 km, dN/dh is well estimated by its value at 1 km:

$$\frac{\mathrm{d}N}{\mathrm{d}h}(1km) = -\frac{312}{7} exp(-1/7) = -38.64 \;\; N - units/km \tag{A.7}$$

When the refractivity gradient displays average characteristics, it is called standard refraction and corresponds to the commonly quoted value of dN_1 = -39 N-units/km. When it becomes positive, it is known as sub-refraction and can cause diffraction loss. When the gradient becomes more negative than dN_1 = -100 N-units/km, it is called super-refractive and results in multipath fading. When it becomes more negative than dN_1 = -157 N-units/km, ducting condition occurs resulting in severe multipath, beam spreading, and even black-out conditions. These refractivity gradients and their corresponding propagation conditions are summarized in Table A.1.

The radio ray is imagined to be straight line relative to an effective Earth's radius, which has been adjusted by the refractivity gradient. This radius is the

real Earth's radius which has been multiplied by an Earth radius factor k that is dependent on the refractivity gradient [34]:

$$k = \frac{r}{R} \tag{A.8}$$

where

k is the effective Earth radius factor,

r is the effective Earth radius and,

R is the true Earth radius.

The ray curvature for various values of k is shown in Fig. A.1.

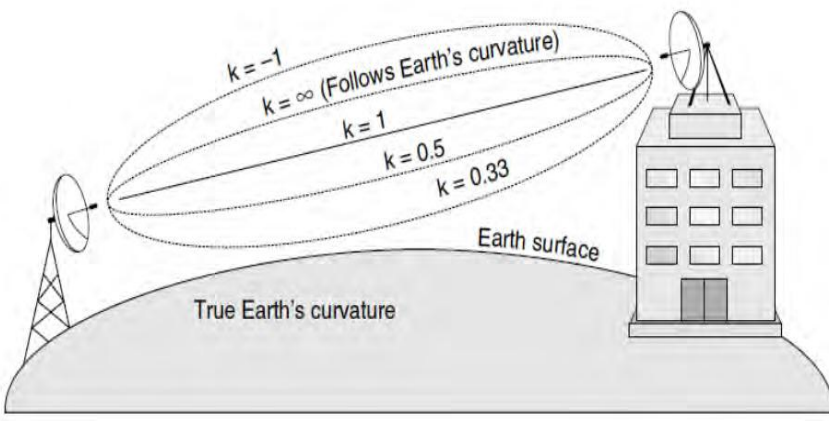

Figure A.1: Variation of the ray curvature for different values of k.

The modified radius are found from the relationship [18]:

$$\frac{\mathrm{d}n}{\mathrm{d}h} + \frac{1}{R} = \frac{1}{r} \tag{A.9}$$

Common radio links, which are described as LOS, incorrectly propose that effective communications are restricted by optical horizon (i.e., $k = 1$). In most circumstances radio links are not restricted to LOS communication. Communications further than the optical horizon can often be realized by some 15%(i.e., $k = 1.33$). That is, the k-factor is related to the refractive index gradient by:

$$k = \frac{1}{1 + R(\frac{\mathrm{d}n}{\mathrm{d}h})} \tag{A.10}$$

where $\frac{\mathrm{d}n}{\mathrm{d}h}$ is the refractive index gradient. From Eq. (A.4) and (A.5), we get

$$\frac{\mathrm{d}n}{\mathrm{d}h} = \frac{\mathrm{d}N}{\mathrm{d}h} \times 10^{-6} = 10^{-6} dN_1 \tag{A.11}$$

So, the value of the k factor is calculated as a function of both the radio refraction gradient and the real Earth radius:

$$k = \frac{1}{1 + 6381(\frac{\mathrm{d}N}{\mathrm{d}h})10^{-6}} = \frac{157}{157 + (\frac{\mathrm{d}N}{\mathrm{d}h})} \tag{A.12}$$

.

Atmospheric Condition	dN_1 **(N-units/km)**	**k Factor**
Normal	-39$\leqslant dN_1 \leqslant$ 0	1 $\leqslant$ k$\leqslant \frac{4}{3}$
Subrefractive	dN_1>0	0$\leqslant$k<1
Super-refractive	-157 <dN_1<-39	k>$\frac{4}{3}$
Ducting	$dN_1\leqslant$-157	k=∞

Table A.1: k factor values for different atmospheric refractive conditions.

As shown in Table A.1, the value of k factor depends on some factors such as refractivity gradient value, refraction type and curvature radius. A commonly used median value for the refractivity gradient of the standard atmosphere is -39 N-units/km, which equals a gradient $\frac{dn}{dh} = 39 \times 10^{-6}$.

Eq. (A.12) brings about an effective Earth radius of k= 1.333 about 4/3. The typical value of 4/3 effective Earth radius is a widely used starting point to characterize atmosphere refractivity for the purposes of radio link planning.

A graph of a Point-to-Point microwave radio link along a path over a terrain profile is shown in Fig A.2. The terrain path profile is a display of the terrain elevations above sea level along the defined path. In this case, the profile has been curved to correspond to a 4/3 effective Earth radius curvature. The radio path between the transmitter and receiver sites is also drawn as a straight line called LOS line. It is labelled as a black line in Fig A.2.

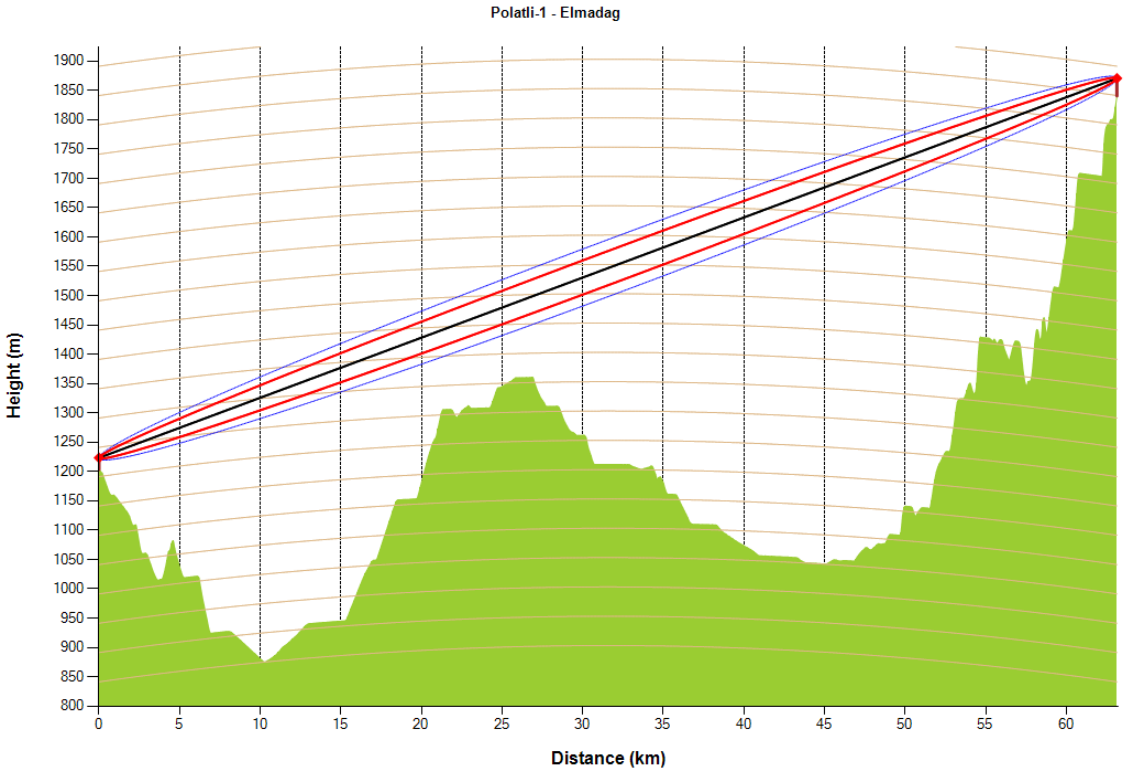

Figure A.2: Polatlı-Elmadag microwave radio link profile over terrain with the terrain elevations above sea level adjusted for 4/3 effective Earth radius curvature. (the blue curve and the red curve indicate the first Fresnel zone and the 0.6 first Fresnel zone, respectively).

Appendix B

Fresnel Zones

Radiowaves travel in a straight line, unless something refracts or reflects them. However, the energy of radiowaves is not pencil thin. So, the radiowaves get from the radiating source can spread out the farther. While radiowaves encounter the obstacles, some portion of their electromagnetic energy penetrate into dark region behind the obstacles due to the diffraction mechanism. Fresnel zones can be thought of reflecting surfaces gives alternating constructive and destructive interference. The geometrical concept of Fresnel zones is shown in Fig. B.1. As shown in Fig. B.1, the Fresnel zones form elliptically shaped solids of revolution around the transmitter-receiver propagation path. The Fresnel zone locus of points exist where [19]

$$d_1 + d_2 + \frac{n\lambda}{2} = a + b \tag{B.1}$$

where number of Fresnel zones are denoted by n. Fig B.1 also illustrates the effect of the n-th Fresnel zone clearance. This clearance is then used as a criterion to de-cide whether an object is to be treated as an obstruction along the path profile. Conceptually, the first Fresnel zone can be thought of as the region where the significant power is transmitted. If the first Fresnel zone is significantly obstructed or blocked, the power available at the receiver can be diminished. A general criterion for link system design is to set the path clearance so that a radius equal to 60% of the first Fresnel zone is unobstructed called *0.6 first Fresnel zone criterion*. From Fig 3.9, the 0.6 first Fresnel zone occurs at a value $v = -0.8$,

which corresponds to the diffraction attenuation of 0.0 dB. In order to calculate the radius of n-th Fresnel zone, the following conditions should be fulfilled:

$$\triangle d = (a+b) - (d_1 + d_2) = \frac{\lambda}{2} \tag{B.2}$$

$$a = \sqrt{r_1^2 + d_1^2} \quad => \quad a \approx d_1[1 + \frac{1}{2}(\frac{r_1}{d_1})^2 + ...] \tag{B.3}$$

$$b = \sqrt{r_1^2 + d_2^2} \quad => \quad b \approx d_2[1 + \frac{1}{2}(\frac{r_1}{d_2})^2 + ...] \tag{B.4}$$

Taking into account that in practical LOS links, r_1 is normally too small in comparison with d_1 and d_2, and ignoring the higher order terms of series of the two last equations, the following equation is given by [19]:

$$r_n \cong \sqrt{\frac{n\lambda d_1 d_2}{d_1 + d_2}} \tag{B.5}$$

where d_1(km) is the distance from transmitting antenna to the point where r_n is calculated, d_2(km) is the distance from receiving antenna to the point where r_n is calculated, λ in meters is the operating wavelength, and n are Fresnel zone numbers.

Similarly, the radius of n-th Fresnel zone can be calculated simply by the following equation [19]:

$$r_n = r_1\sqrt{n} \tag{B.6}$$

As shown in Fig. B.2, an approximate formula [7, 35] for calculating the first Fresnel zone radius, F_1 is given by:

$$F_1 = 17.3\sqrt{\frac{d_1 d_2}{f(d_1 + d_2)}} \tag{B.7}$$

where F_1 is the first Fresnel radius in metres, d_1 (km) and d_2 (km) are the distances of the obstacles from transmitting and receiving antennas, respectively and f is the radio frequency in GHz.

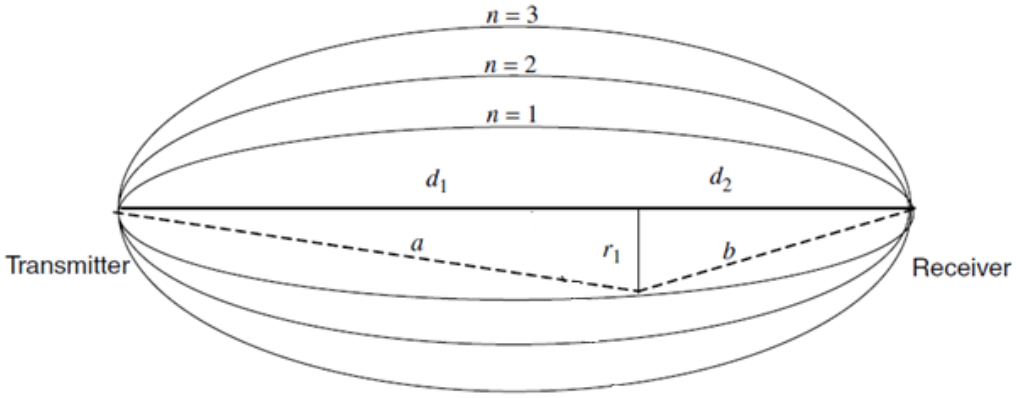

Figure B.1: Geometrical concept of Fresnel zones.

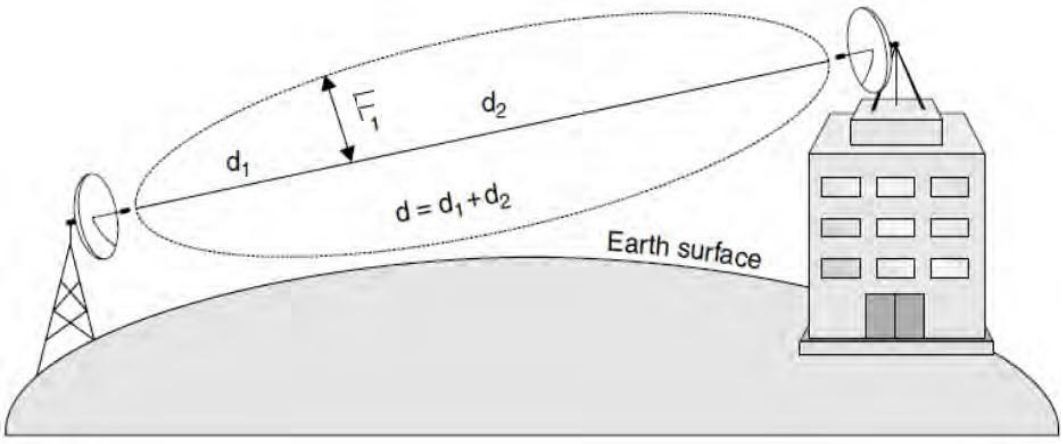

Figure B.2: An illustration of the first Fresnel zone radius.

Bibliography

[1] K. Morita, "Prediction of Rayleigh fading occurrence probability of line-of-sight microwave links," *Rev. Elec. Commun. Lab.*, vol. 18, pp. 810–821, Nov.-Dec. 1970.

[2] W. T. Barnett, "Multipath propagation at 4, 6 and 11 GHz," *Bell System Technical Journal*, vol. 51, no. 2, pp. 321–361, February 1972.

[3] A. Vigants, "Space diversity engineering," *Bell System Technical Journal*, vol. 54, no. 1, pp. 103–142, January 1975.

[4] R. L. Olsen and T. Tjelta, "Worldwide techniques for predicting the multipath fading distribution on terrestrial LOS links: Background and results of tests," *IEEE Transactions on Antennas and Propagation*, vol. 47, no. 1, pp. 157–170, January 1999.

[5] R. L. Olsen and T. Tjelta, "Worldwide techniques for predicting the multipath fading distribution on terrestrial LOS links: Comparison with regional techniques," *IEEE Transactions on Antennas and Propagation*, vol. 51, no. 1, pp. 23–30, January 2003.

[6] Recommendation ITU-R P.530-8, "Propagation data and prediction methods required for the design of terrestrial line-of-sight systems," *International Telecommunication Union, Geneva*, 1999.

[7] Recommendation ITU-R P.530-15, "Propagation data and prediction methods required for the design of terrestrial line-of-sight systems," *International Telecommunication Union, Geneva*, 2013.

[8] *ATDI ICS telecom software platform.* http://www.atdi.com/ics-telecom/.

[9] M. Kvicera, *et al.*, "Short-term terrain diffraction measurements: Preliminary results," in *Proceedings of European Conference on Antenna and Propagation-7th Eur. Conf. Antennas. Propag.*, Gothenburg, April 2013, pp. 52-55.

[10] M. Kvicera, *et al.*, "Short-term terrain diffraction measurements from L- to Q-Band: Results and Analysis," *IEEE Transactions on Antennas and Propagation*, vol. 62, no. 7, pp. 3693–3701, July 2014.

[11] H. R. Anderson, *Fixed Broadband Wireless System Design.* John Wiley & Sons Ltd., 2003.

[12] B. L. Agba, *et al.*, "Comparison of microwave links prediction methods: Barnett-Vigants vs. ITU methods," in *Proceedings of Progress In Electromagnetics Research Symposium,*, Xi'an, China, March 22-26 2010.

[13] K. T. Vieira, "Comparisons of Barnett-Vigants method with ITU-R link data base," tech. rep., EAB/G-03:002609 Uae Ericssonwide Internal Report, August 2003.

[14] T. Tjelta *et al.*, "Systematic development of new multivariable techniques for predicting the distribution of multipath fading on terrestrial microwave links," *IEEE Transactions on Antennas and Propagation*, vol. 38, no. 10, pp. 1650-1665, October 1990.

[15] B. L. Agba, *et al.*, "Recent evolution of ITU method for prediction of multipath fading on terrestrial microwave links," in *Proceedings of Progress In Electromagnetics Research Symposium, Marrakesh*, Morocco, March 20-23 2011.

[16] D. Sayed, *et al.*, "Comparison between the actual microwave terrestrial links performance and different models," in *Third International Conference on Sensor Technologies and Applications,*, 2009.

[17] P. Goktas, A. Altintas, S. Topcu and E. Karasan, "The effect of terrain roughness in the microwave line-of-sight multipath fading estimation based

on Rec. ITU-R P.530-15," in *General Assembly and Scientific Symposium (URSI GASS), 2014 XXXIth URSI*, China, August 2014.

[18] Recommendation ITU-R P.453, "The radio refractivity index: its formula and refractivity data," *International Telecommunication Union, Geneva*, 2012.

[19] Recommendation ITU-R P.526, "Propagation by diffraction," *International Telecommunication Union, Geneva*, 2013.

[20] Recommendation ITU-R P.676, "Attenuation by atmospheric gases," *International Telecommunication Union, Geneva*, 2012.

[21] J. S. Seybold, *Introduction to RF Propagation*. John Wiley & Sons Ltd., 2005.

[22] Recommendation ITU-R P.837, "Characteristics of precipitation for propagation modelling," *International Telecommunication Union, Geneva*, 2012.

[23] Recommendation ITU-R P.838, "Specific attenuation model for rain for use in prediction methods," *International Telecommunication Union, Geneva*, 2005.

[24] P. Angueira and J. A. Romo, *Microwave Line of Sight Link Engineering*. John Wiley & Sons Ltd., 2012.

[25] T. S. Rappaport, *Wireless Communications: Principles and Practice (2nd Edition)*. ser. Prentice Hall Communications Engineering and Emerging Technoligies series, Prentice Hall Inc., 2002.

[26] K. Bullington, "Radio propagation at frequencies above 30 Megacycles," *Proceedings of the Institute of Radio Engineers*, vol. 35, pp. 1122-1136, October 1947.

[27] J. Epstein and D. W. Peterson, "An experimental study of wave propagation at 850 Mc/s," *Proceedings of the Institute of Radio Engineers*, vol. 41, pp. 595-611, May 1953.

[28] J. Deygout, "Multiple knife-edge diffraction of microwaves," *IEEE Transactions on Antennas and Propagation*, vol. 14, pp. 480-489, July 1966.

[29] Recommendation ITU-R P.527, "Electrical characteristics of the surface of the Earth," *International Telecommunication Union, Geneva*, 1992.

[30] ITU Report 1008-1, "Reflection from the surface of the Earth," *International Telecommunication Union, Geneva*, 1990.

[31] L. Harvey, *Microwave Transmission Networks: Planning, Design and Deployment*. McGraw Hill, New York, 2010.

[32] MIL-PRF-89020A, *Performance Specification Digital Terrain Elevation Data*, 1996.

[33] Recommendation ITU-R P.452, "Prediction procedure for the evaluation of interference between stations on the surface of the earth at frequencies above about 0.1 GHz," *International Telecommunication Union, Geneva*, 2013.

[34] T. Manning, *Microwave Radio Transmission Design Guide*. Artech House, 2009.

[35] R. L. Freeman, *Radio System Design for Telecommunications*. John Wiley & Sons Ltd., 1997.